

RESEARCH ARTICLE

Glucuronoxylomannan intranasal challenge prior to *Cryptococcus neoformans* pulmonary infection enhances cerebral cryptococcosis in rodents

Hiu Ham Lee¹, Dylan J. Carmichael¹, Victoria Ribeiro², Dana N. Parisi^{1,3}, Melissa E. Munzen⁴, Claudia L. Charles-Niño⁴, Mohamed F. Hamed^{4,5}, Ettiman Kaur⁶, Ayush Mishra⁶, Jiya Patel⁶, Rikki B. Rooklin⁶, Amina Sher⁶, Maria A. Carrillo-Sepulveda¹, Eliseo A. Eugenin², Michael R. Dores⁶, Luis R. Martinez^{1,3,4,7,8,9*}



OPEN ACCESS

Citation: Lee HH, Carmichael DJ, Ribeiro V, Parisi DN, Munzen ME, Charles-Niño CL, et al. (2023) Glucuronoxylomannan intranasal challenge prior to *Cryptococcus neoformans* pulmonary infection enhances cerebral cryptococcosis in rodents. PLoS Pathog 19(4): e1010941. <https://doi.org/10.1371/journal.ppat.1010941>

Editor: Maurizio Del Poeta, Stony Brook University, UNITED STATES

Received: October 21, 2022

Accepted: April 17, 2023

Published: April 28, 2023

Copyright: © 2023 Lee et al. This is an open access article distributed under the terms of the [Creative Commons Attribution License](https://creativecommons.org/licenses/by/4.0/), which permits unrestricted use, distribution, and reproduction in any medium, provided the original author and source are credited.

Data Availability Statement: All relevant data are within the manuscript and its [Supporting Information](#) files.

Funding: M.E.M., C.L.C.-N., M.F.H., M.R.D., and L.R.M. were supported by the National Institute of Allergy and Infectious Diseases (NIAID award # R01AI145559) of the US National Institutes of Health (NIH). E. A. E. was supported by the National Institute of Mental Health (NIMH award # MH096625 and MH128082) of the US NIH, the

1 Department of Biomedical Sciences, NYIT College of Osteopathic Medicine, New York Institute of Technology, Old Westbury, New York, United States of America, **2** Department of Neuroscience, Cell Biology, and Anatomy, The University of Texas Medical Branch, Galveston, Texas, United States of America, **3** Department of Biomedical Sciences, Long Island University-Post, Brookville, New York, United States of America, **4** Department of Oral Biology, University of Florida College of Dentistry, Gainesville, Florida, United States of America, **5** Department of Pathology, Faculty of Veterinary Medicine, Mansoura University, Mansoura, Egypt, **6** Department of Biology, Hofstra University, Hempstead, New York, United States of America, **7** Emerging Pathogens Institute, University of Florida, Gainesville, Florida, United States of America, **8** Center for Immunology and Transplantation, University of Florida, Gainesville, Florida, United States of America, **9** Center for Translational Research in Neurodegenerative Disease, University of Florida, Gainesville, Florida, United States of America

* LMartinez@dental.ufl.edu

Abstract

The encapsulated fungus *Cryptococcus neoformans* is the most common cause of fungal meningitis, with the highest rate of disease in patients with AIDS or immunosuppression. This microbe enters the human body via inhalation of infectious particles. *C. neoformans* capsular polysaccharide, in which the major component is glucuronoxylomannan (GXM), extensively accumulates in tissues and compromises host immune responses. *C. neoformans* travels from the lungs to the bloodstream and crosses to the brain via transcytosis, paracytosis, or inside of phagocytes using a “Trojan horse” mechanism. The fungus causes life-threatening meningoencephalitis with high mortality rates. Hence, we investigated the impact of intranasal exogenous GXM administration on *C. neoformans* infection in C57BL/6 mice. GXM enhances cryptococcal pulmonary infection and facilitates fungal systemic dissemination and brain invasion. Pre-challenge of GXM results in detection of the polysaccharide in lungs, serum, and surprisingly brain, the latter likely reached through the nasal cavity. GXM significantly alters endothelial cell tight junction protein expression *in vivo*, suggesting significant implications for the *C. neoformans* mechanisms of brain invasion. Using a microtiter transwell system, we showed that GXM disrupts the trans-endothelial electrical resistance, weakening human brain endothelial cell monolayers co-cultured with pericytes, supportive cells of blood vessels/capillaries found in the blood-brain barrier (BBB) to promote *C. neoformans* BBB penetration. Our findings should be considered in the

National Institute of Neurological Disorders and Stroke (NINDS award # NS105584) of the US NIH, and The University of Texas Medical Branch internal funding. The funders had no role in the study design, data collection and analysis, decision to publish, or preparation of the manuscript.

Competing interests: The authors have declared that no competing interests exist.

development of therapeutics to combat the devastating complications of cryptococcosis that results in an estimated ~200,000 deaths worldwide each year.

Author summary

Cryptococcus neoformans infection of the central nervous system (CNS) typically begins by inhalation of fungal spores and results in devastating mortality rates worldwide. Over 200,000 deaths have been reported annually, with cryptococcal meningoencephalitis being the most severe form of the disease. This study investigates the ability of the fungus to invade, colonize, and cause damage to the host through properties of the fungal polysaccharide capsule, which allows the microbe a variety of both protective and offensive abilities. This capsule, made primarily of the polysaccharide glucuronoxylomannan (GXM), has been implicated in the progression and severity of cryptococcal infection in the CNS. We determined that GXM increases the fungal burden in the lungs of mice and enhances fungal migration to the brain. Interaction of GXM with the blood-brain barrier, which is a protective structure that regulates movement of particles into the CNS, demonstrated that GXM can disrupt the integrity of this barrier, compromising the delicate balances of fluids, immune cells, and other factors vital to the maintenance of the CNS. The findings of this study reveal the substantial role of GXM in establishing *C. neoformans* infection in the brain and necessitate future studies to further understand these interactions.

Introduction

Cryptococcus neoformans is an encapsulated opportunistic yeast-like fungus responsible for life-threatening meningoencephalitis in both immunocompromised and previously healthy individuals. Cryptococcosis is responsible for an estimated 200,000 deaths per year globally [1], especially in HIV infected patients. *C. neoformans* initially infects humans during early childhood [2] through inhalation of small fungal particles in the form of desiccated or poorly encapsulated yeast or basidiospores [3,4]. In most immunocompetent hosts, the fungus is controlled by local host responses and remains dormant in the lungs. However, reactivation can occur by immunosuppression, resulting in fungal replication in the lungs followed by dissemination via the bloodstream or lymphatic system to other organs, especially the brain. During cryptococcosis, fungemia is detected in about 50% of HIV-infected patients [5]. The correlation between fungemia and dissemination, including brain invasion, has been utilized for the development of experimental models of cryptococcosis [6], and fungemia is identified as an independent parameter of early mycological failure in humans [5]. *C. neoformans* crosses the blood-brain barrier (BBB) [7] by transcytosis, paracytosis, or via a “Trojan horse” mechanism by being transported within host inflammatory cells [8]. Once the fungus reaches the brain, it can cause lethal meningoencephalitis, which is the most serious pathological manifestation of cryptococcosis.

Microbial pathogenesis depends on the ability of the host to combat infection. Microbes like *C. neoformans* have specific virulence factors, including melanin production, the ability to grow at mammalian temperatures, and the polysaccharide capsule, that allow them to evade multiple immune defenses and damage the host. The capsule of *C. neoformans* is the most distinctive physical structure of the cryptococcal cell, located outside the cell wall [9,10]. This

structure may protect the fungus from changes in the environment such as desiccation or against predation by soil amoeba [11]. The capsule is composed of at least three components: glucuronoxylomannan (GXM), galactoxylomannan, and mannoprotein, with GXM being its major constituent. Genetic and molecular biology strategies have shown that the capsule is a major contributor to *C. neoformans* infection since non-encapsulated strains have reduced virulence [12]. Immunocompromised individuals with cryptococcosis typically have high levels of *C. neoformans* capsular polysaccharide (CPS) in their serum and cerebrospinal fluid (CSF) [13,14]. Furthermore, the extensive accumulation of GXM in tissue is believed to be a major contributor to *C. neoformans* pathogenesis. This compound has been associated with a variety of immunosuppressive effects [15], such as interference with phagocytosis, antigen presentation, leukocyte migration and proliferation, as well as impediment of specific antibody (Ab) responses. GXM also enhances HIV replication [16]. However, there is lack of information on the role of *C. neoformans* GXM on lung dissemination into the bloodstream and brain invasion or pathogenesis.

Immunohistochemical analysis of post-mortem individuals' brains with cryptococcosis exhibited substantial levels of GXM released around large penetrating vessels [17] suggesting an important role of this carbohydrate on central nervous system (CNS) invasion by this fungus. In fact, *C. neoformans* sheds large amounts (range μg to mg/mL) of polysaccharide into the CSF and infected tissues [14]. In this study, we challenged C57BL/6 mice with exogenous purified GXM before pulmonary infection with cryptococci and compared these mice to animals that were not sensitized with the polysaccharide. We found that exogenous GXM reaches the CNS, exacerbates fungal pulmonary disease, enhances *C. neoformans* dissemination from the lungs to the CNS, and has detrimental effects on tight junction proteins (TJs), the molecules that regulate endothelial cells in the BBB. These observations suggest that GXM intranasal (i.n.) challenge prior to *C. neoformans* pulmonary infection enhances brain invasion and colonization in rodents via disruption of the TJs on endothelial cells of the BBB.

To investigate the disruption of BBB integrity by GXM, we measured the activation of RhoA, a member of the Ras-related small GTPase Rho family that signals to regulate the actin cytoskeleton [18]. When bound to GTP, RhoA functions as a regulatory switch that confers increased endothelial cell permeability [19] and BBB disruption [20]. We found that GXM-induced RhoA signaling to myosin-light chain (MLC) is significant and time-dependent, and demonstrated morphological changes in the actin cytoskeleton of cells treated with GXM. Our observations suggest that remodeling of the actin cytoskeleton in endothelial cells may be a mechanism of virulence for *C. neoformans* to cross the BBB and establish infection in the brain. These findings complement our *in vitro* observations that GXM alters BBB permeability and contributes to increased fungal transmigration into the brain.

Results

GXM concentrations in murine tissues 24 h post-administration

To explore the impact of exogenous GXM on *C. neoformans* H99 strain infection, we first determined whether GXM disseminated systemically from the airways and could be detected in serum and brain tissue (Table 1). Therefore, C57BL/6 mice ($n = 5$) were challenged i.n. with a single GXM dose of $125 \mu\text{g/mL}$, and the CPS levels were quantified by enzyme-linked immunosorbent assay (ELISA) 24 h later. We selected this GXM concentration ($125 \mu\text{g/mL}$) to sensitize the mice because the capsular material disseminates throughout the mouse body (e.g., lungs, serum, and brain) at final allowable physiological organ/serum concentrations comparable to previous studies [14] and because a similar dose induces immunological unresponsiveness [21]. Lung tissue GXM levels were $2.17 \pm 0.09 \mu\text{g/g}$. We also examined whether i.n.

Table 1. GXM levels in tissues of C57BL/6 mice ($n = 5$) 24 h post-intranasal administration.

Tissue	GXM concentration*
Brain	$0.21 \pm 0.13 \mu\text{g/g}$
Lung	$2.17 \pm 0.09 \mu\text{g/g}$
Serum	$0.34 \pm 0.05 \mu\text{g/mL}$

*The background levels of the ELISA readings for the excised organs and withdrawn sera from the negative control mice (no GXM administration) were on average 0.06. GXM was undetected in these samples.

<https://doi.org/10.1371/journal.ppat.1010941.t001>

exogenous GXM administration in C57BL/6 mice resulted in pulmonary inflammation after 24 h to understand its impact in *C. neoformans* infection (S1 Fig). Mice i.n. administered with phosphate-buffered saline (PBS; untreated) displayed lungs with a normal interstitial tissue and clear alveolar throughout the pulmonary lobe (S1 Fig). Lower magnification (10-20X) images of untreated pulmonary tissue exhibited low to moderate activated alveolar macrophages. Higher magnification images (40-100X) demonstrated alveoli with slightly thickened septa (red arrow) and activated alveolar macrophages with abundant large eosinophilic cytoplasm (blue arrowhead). In contrast, lungs removed from GXM-treated mice exhibited slight inflammation with diffuse thickening of the interalveolar tissue and active hyperemia in the pulmonary lobule (S1 Fig). Lower magnification (10-20X) images showed emphysematous alveoli with atelectasis (green arrow; complete or partial collapse of a lung area) and thickening of the interalveolar septa. A closer look (40-100X) to the pulmonary tissue revealed thickening and hyalinization of interalveolar septa, and considerably congested blood capillaries with reactive endothelial lining (yellow arrowhead). GXM concentrations in serum and brain tissue were $0.34 \pm 0.05 \mu\text{g/mL}$ and $0.21 \pm 0.13 \mu\text{g/g}$, respectively. As a control experiment, we measured the GXM levels in lungs, serum, and brain collected from mice only infected with the fungus intratracheally (i.t.; no GXM challenge) 3- and 7-days post-infection (dpi; S2 Fig). The levels of GXM in pulmonary tissue 3- and 7-dpi were the highest with 13.6 (range: 10 to 18 $\mu\text{g/g}$) and 17.9 (range: 13 to 22 $\mu\text{g/g}$) $\mu\text{g/g}$, respectively. Brain tissue evinced GXM concentrations of 4.4 (range: 2 to 7 $\mu\text{g/g}$, 3-dpi) and 12.8 (range: 9 to 19 $\mu\text{g/g}$, 7-dpi) $\mu\text{g/g}$. Additionally, circulating GXM in serum was 4.75 (range: 2 to 7 $\mu\text{g/mL}$, 3-dpi) and 10.25 (range: 7 to 14 $\mu\text{g/mL}$, 7-dpi) $\mu\text{g/mL}$. Therefore, this control experiment shows that GXM accumulation in tissues and serum during a typical i.t. infection is comparable to previous reports in the field of cryptococcosis. These measurements validated that GXM delivered into the nasal cavity can be detected in tissues other than the lungs, causes inflammation of the pulmonary tissue, and its concentrations reach sub-physiological levels in tissue and serum.

Pre-conditioning with GXM exacerbates murine cryptococcosis and mortality

We investigated the impact of GXM prior to C57BL/6 infection with *C. neoformans* H99 strain cells (Fig 1). Mice were sensitized i.n. with 125 $\mu\text{g/mL}$ of GXM 24 h pre-inoculation with 10^5 *C. neoformans* yeast cells (Fig 1A). Cryptococcosis progression was compared between these mice and rodents infected with the fungus only (untreated). i.n. administration of GXM significantly accelerated the death of *C. neoformans*-infected mice relative to control mice ($n = 10$ mice per group; $P < 0.001$; Fig 1B). On day 16 post-infection, 100% of GXM-treated mice had died compared to 20% of untreated mice. On average, GXM-treated mice died 12-dpi, whereas untreated mice died 22-dpi (Fig 1B). These findings indicate that i.n. GXM sensitization enhances mortality in mice upon pulmonary infection.

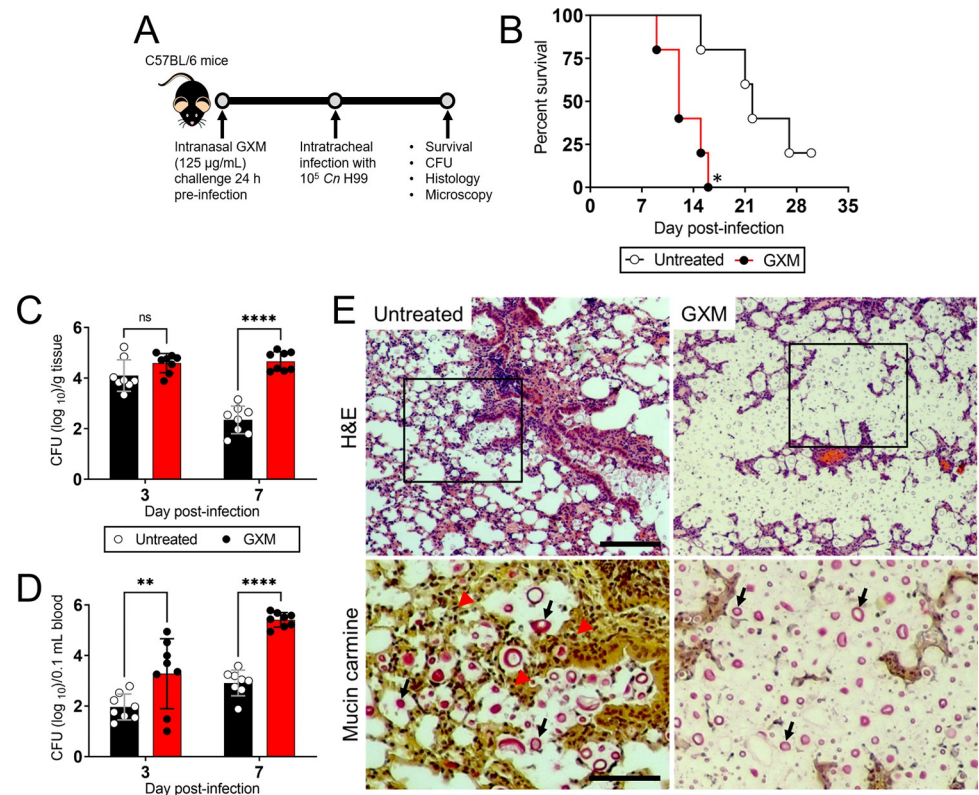


Fig 1. Exogenous glucuronoxylomannan (GXM) administration and *Cryptococcus neoformans* H99 strain pulmonary infection reduces survival in C57BL/6 mice. (A) Experimental timeline for the intranasal (i.n.) GXM challenge and fungal intratracheal (i.t.) infection model. Mice were sensitized with 125 $\mu\text{g}/\text{mL}$ of GXM 24 h pre-inoculation with 10^5 *C. neoformans* cells. Then, survival studies and colony forming units (CFU) determinations, histopathology, and microscopy were performed 3- and 7-days post-infection (dpi). The C57BL/6 mouse cartoon in the timeline is a creative commons clip art inserted using Microsoft Office Power Point 2019. This diagram was drawn by Luis R. Martinez. (B) Survival differences of untreated (e.g., sterile phosphate-buffered saline (PBS)-sensitization) and GXM-treated C57BL/6 mice infected with 10^5 fungi ($n = 10$ per group). P -value significance ($* P < 0.05$) was calculated by log rank (Mantel-Cox) analysis. Fungal burden in (C) lungs (numbers of CFU/gram (g) of tissue) and (D) blood (numbers of CFU/0.1 mL of blood) collected from untreated and GXM-treated mice i.t. infected with 10^5 cryptococci ($n = 8$ per group) 3- and 7-dpi. For panels C and D, bars denote the means and standard deviations (SDs), respectively. Asterisks indicate P -value significance (** $P < 0.01$ and **** $P < 0.0001$) calculated using multiple student's t -test analyses. ns represents not statistically significant comparisons. For panels A–D, these experiments were performed twice, similar results were obtained each time, and all the results combined are presented. (E) Histological analysis of lungs removed 7-dpi from untreated (left panels) and GXM-treated (right panels) C57BL/6 mice infected with 10^5 *C. neoformans* H99 strain cells. Representative hematoxylin and eosin (H&E), host tissue morphology; upper panels; Scale bar: 100 μm)- and mucin carmine (fungi; red staining; lower panels)-stained sections of the lungs sequentially examined are shown. Lower panel images are magnifications of the smaller boxes in the H&E-stained sections to better show the cryptococcal cells stained with mucin carmine (indicated with arrows; Scale bar: 20 μm).

<https://doi.org/10.1371/journal.ppat.1010941.g001>

We quantified *C. neoformans* pulmonary burden in untreated and GXM-treated mice 3- and 7-dpi. Although we did not observe cryptococcal load differences between untreated [4.1×10^4 colony forming units (CFU)] and GXM (4.59×10^4 CFU)-challenged rodents 3-dpi (Fig 1C), we demonstrated that the difference in pulmonary fungal burden was evident 7-dpi, with GXM-treated animals (4.66×10^4 CFU) having a significantly higher burden than untreated mice (2.35×10^2 CFU; $P < 0.0001$; Fig 1C). Interestingly, untreated mice infected with cryptococci showed a considerable reduction in fungal load 7-dpi (4.1×10^4 CFU) relative to 3-dpi (2.35×10^2 CFU). Hematoxylin and eosin (H&E) staining of pulmonary tissue removed from

untreated mice 7-dpi evinced localized inflammation and dense cellular infiltration around aggregates or individual cryptococci (Fig 1E; left upper panel; 20X). Mucine carmine staining of magnified lung tissue from untreated rodents showed *C. neoformans* cells (black arrows) of diverse sizes surrounded by inflammatory cells (red arrowheads) with limited or contained CPS production particularly around individual aggregates or individual cryptococci (Fig 1E; left lower panel; 40X). In contrast, lungs excised from GXM-treated mice exhibited high fungal burden characterized by large numbers of cryptococci embedded in abundant amounts of CPS with little inflammation (Fig 1E; right upper [20X] and lower [40X] panels). In addition, cryptococci was more extensively found in the blood and brain of GXM-treated mice when compared to the untreated group (Fig 1D). These results suggest that GXM dysregulates host homeostasis and enhances disease by increasing pulmonary fungal burden, inhibiting host inflammation, facilitating the access of cryptococci to the bloodstream, and enhancing fungal dissemination to the CNS.

GXM facilitates *C. neoformans* dissemination from the lungs to the CNS

We investigated the impact of exogenous GXM administration on *C. neoformans* dissemination to the brain (Fig 2). We demonstrated that brain fungal load in GXM-treated animals (3-dpi, 2.45×10^2 CFU; 7-dpi, 5.03×10^5 CFU) were significantly higher than in untreated (3-dpi, 1.67×10^1 CFU; 7-dpi, 1.94×10^1 CFU) mice (3-dpi, $P < 0.05$; 7-dpi, $P < 0.0001$; Fig 2A). Immunofluorescence (IF) staining and confocal microscopy of *C. neoformans*-infected brain tissue 7-dpi showed cryptococci of different size (yellow arrowheads) embedded in neuronal tissue (Fig 2B). A 7-dpi tissue section of the dentate gyrus in the hippocampus of a GXM-challenged mouse exhibited a large cryptococcoma (red arrows) filled with yeasts cells (yellow arrowhead) and substantial amounts of capsular GXM released (white arrowheads) (Fig 2C). Extensive accumulation of GXM (white arrowheads) was also observed in cortical tissue (Fig 2D) and a large blood vessel (Fig 2E) in the brain parenchyma of GXM-treated and *C. neoformans*-infected mice 7-dpi. In addition, 7-dpi IF staining showed a significantly higher number of lesions in the brains of GXM-treated mice (average, 7.86 ± 0.91) than those of untreated animals (2.43 ± 0.43) ($P < 0.001$) (Fig 2F–2H). The average areas of brain lesions of GXM-treated infected mice reached $241 \mu\text{m}^2 \pm 27.79$, whereas lesions of control mice averaged $166 \mu\text{m}^2 \pm 75$ ($P < 0.05$) (Fig 2I). These studies demonstrate that exogenous GXM administration increases the permeability of the CNS to *C. neoformans* invasion and colonization.

GXM reduces the expression of TJ proteins in mouse brain tissue

To confirm that GXM reached the CNS of challenged uninfected mice (7.8 to 125 $\mu\text{g}/\text{mL}$; PBS-instilled animals were used as controls, untreated) 24 h after i.n. administration, IF staining using GXM-specific monoclonal Ab (mAb) 18B7 demonstrated fungal polysaccharide (green) distribution (white arrowheads) throughout the brain parenchyma 24 h after administration (Fig 3A). During pathologic conditions, TJ disruptions promote enhanced leukocyte adhesion to, and transmigration across, CNS vessels [22], resulting in BBB permeability and parenchymal leukocyte accumulation [23,24]. Presently, studies dealing with the effects of GXM on the expression of TJs in the mouse brain are scarce. TJ proteins provide essential structural support to the BBB playing an important role in maintaining a safe neural microenvironment in the brain. Using Western blot (WB) analysis (Fig 3B), we found that GXM administration prior to *C. neoformans* pulmonary infection alters specific TJ expression in the mouse brain. GXM doses $\geq 62.5 \mu\text{g}/\text{mL}$ decrease the expression of claudin-5 (Fig 3C), ZO-1 (Fig 3D), and JAM-A (Fig 3F; $P < 0.05$) in brain tissue. Interestingly, occludin downregulation was observed

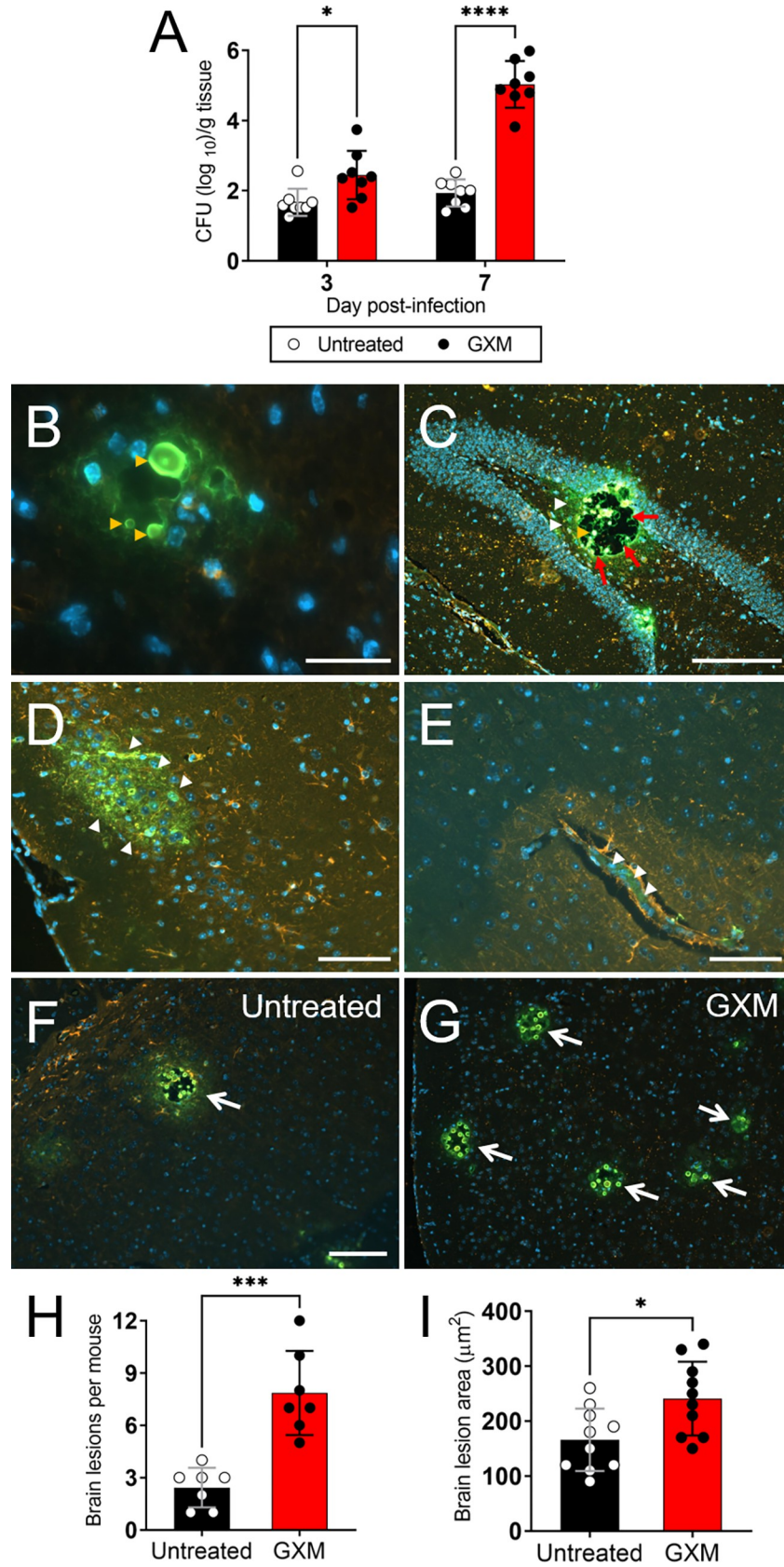


Fig 2. Exogenous GXM challenge enhances *C. neoformans* migration into the central nervous system (CNS) of C57BL/6 mice. (A) Fungal burden (numbers of CFU/gram of tissue) in brain collected from untreated and GXM-treated mice i.t. infected with 10^5 cryptococci ($n = 8$ per group) 3- and 7-dpi. (B) Confocal microscopy of cryptococcal cells (yellow arrowheads) in the brain parenchyma of GXM-treated mice 7-dpi. Scale bar: 20 μm . (C) Immunofluorescent (IF) image of a 7-dpi hippocampal tissue section displaying a large cryptococcoma (red arrows) filled with yeasts cells (yellow arrowhead) and abundant amounts of capsular polysaccharide released (white arrowheads). Scale bar: 150 μm . (D) GXM accumulation (white arrowheads) in the cortex and (E) blood vessel of GXM-treated and *C. neoformans* infected mice 7-dpi. Scale bar: 200 μm . IF staining of brain lesions (cryptococcomas; white arrows) caused by *C. neoformans* 7-dpi in (F) untreated or (G) GXM-treated animals. Scale bar: 150 μm . For B to G, FITC-labeled (green) GXM-specific monoclonal antibody (mAb) 18B7 was used to label cryptococci. MAP-2 (red) and DAPI (blue) staining were used to label the cell bodies and nuclei of neurons, respectively. Each tissue section was sequentially examined using multiple slides. (H) Brain lesions per mouse ($n = 7$ per group) and (I) lesion area ($n = 10$ per group) analyses in tissue sections of untreated and GXM-treated mice infected with *C. neoformans*. The areas of 10 brain lesions per condition were measured using NIH ImageJ software. Each symbol represents a single lesion. For A, H and I, bars and error bars denote the mean value and SDs, respectively. Asterisks denote *P*-value significance (* $P < 0.05$, *** $P < 0.001$, and **** $P < 0.0001$) calculated using single or multiple student's *t*-test analyses.

<https://doi.org/10.1371/journal.ppat.1010941.g002>

in rodent brains challenged with GXM doses $\geq 15.6 \mu\text{g/mL}$ (Fig 3E). Our data suggest that GXM-induced TJ protein reduction may be a major cause of profound brain alterations including an increase in susceptibility of the CNS to cryptococcal infection.

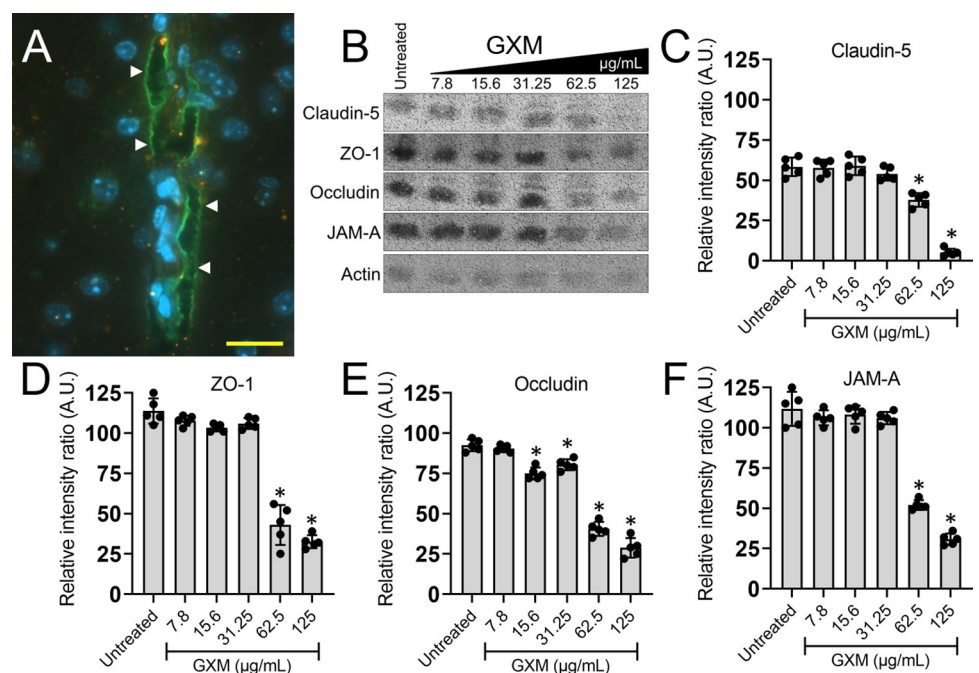


Fig 3. GXM challenge alters tight junction protein (TJ) expressions *in vivo*. (A) Confocal microscopy of cryptococcal GXM [FITC-labeled (green; arrowheads) GXM-specific mAb 18B7] distribution in the brain parenchyma (blue; nuclei of neurons) of GXM (125 $\mu\text{g/mL}$)-treated mice 24 h after i.n. administration. Scale bar: 20 μm . (B) Western blot (WB) analyses of brain tissue from untreated (e.g., sterile PBS-sensitized) or GXM (7.8, 15.6, 31.25, 62.5, and 125 $\mu\text{g/mL}$)-challenged C57BL/6 mice were performed to compare the expression of the TJ proteins claudin-5 (23 kDa), ZO-1 (200 kDa), and occludin (59 kDa) and the adhesion protein JAM-A (32 kDa). Actin (42 kDa) was used as a housekeeping protein control. Quantitative measurements of individual band intensity in WB analyses described in panel B for (C) claudin-5, (D) ZO-1, (E) occludin, and (F) JAM-A, using NIH ImageJ software. Actin was used as a control to determine the relative intensity ratio (A.U. denotes arbitrary units). Bars represent the means of 5 independent gel results (black circles) and error bars indicate SDs. Asterisks denote *P*-value significance calculated using one-way analysis of variance (ANOVA) and adjusted using the Tukey's post-hoc analysis. * $P < 0.05$, for the reduction in the intensity of the band of TJ and adhesion molecules as compared to actin.

<https://doi.org/10.1371/journal.ppat.1010941.g003>

GXM alters the distribution/intensity of TJs on human brain endothelial cells (HBECs)

To validate the results obtained in the murine model and to determine the impact of GXM on TJs, we analyzed the distribution of TJs (claudin-5 and occludin) in HBECs after exposure to the capsular component for 4 h using IF microscopy (Fig 4). The distribution of claudin and occludin on HBECs is considerably reduced after incubation with 10 $\mu\text{g}/\text{mL}$ of GXM (Fig 4A). We chose this GXM concentration (10 $\mu\text{g}/\text{mL}$) for most of our *in vitro* experiments because it matches the mouse serum levels described by others [25,26] and was confirmed in these studies 7-dpi (S2 Fig). Ethylenediaminetetraacetic acid (EDTA; 10 $\mu\text{g}/\text{mL}$) was used as a positive control [27] and, similarly to GXM, substantially decreased the distribution of TJs on the surface of HBECs. Quantification of claudin-5 intensity on HBECs using the NIH ImageJ software demonstrated that GXM ($P < 0.01$) and EDTA ($P < 0.0001$) significantly reduced this TJ intensity relative to untreated control HBECs (Fig 4B). There were no differences in the distribution of claudin-5 in HBECs incubated with EDTA or GXM. Occludin intensity was also significantly decreased in HBECs cultured with GXM ($P < 0.05$) or EDTA ($P < 0.0001$) compared to untreated cells (Fig 4C). Similarly, EDTA-treated HBECs evinced lower occludin intensity on their surfaces than GXM-treated cells ($P < 0.01$). These experiments indicate that the distribution/intensity of TJs on HBECs is reduced after incubation with GXM.

GXM increases the expression of RhoA cytoskeletal regulator in a time-dependent manner

A previous study demonstrated that *C. neoformans* activates Rho GTPases to promote transmigration across a HBEC monolayer *in vitro*, which is the critical step for cryptococcal brain

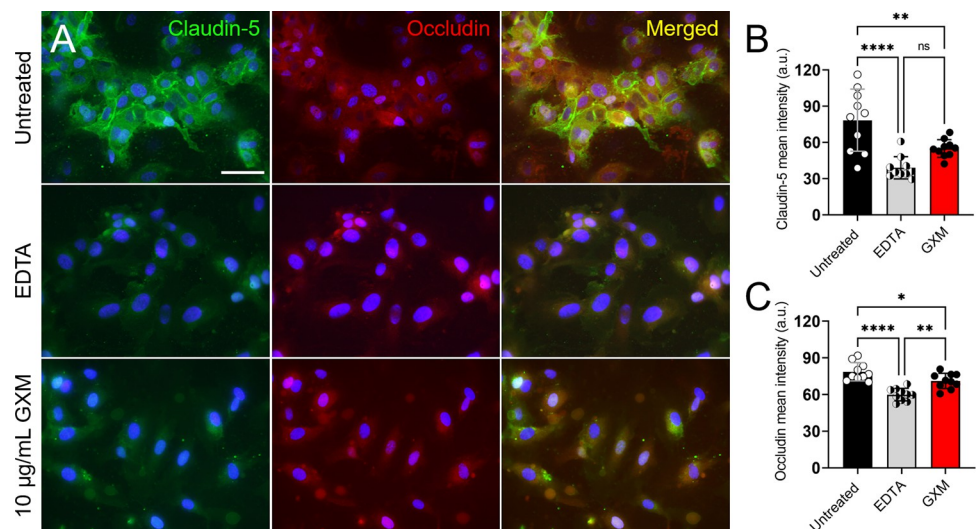


Fig 4. GXM alters the distribution of TJs on human brain endothelial cells (HBECs). (A) IF images of claudin-5 and occludin distribution on the surface of HBECs after incubation in absence (untreated) and presence of 10 $\mu\text{g}/\text{mL}$ of ethylenediaminetetraacetic acid (EDTA; positive control) or GXM for 4 h at 37°C and 5% CO_2 . After co-incubation with EDTA or GXM, the cells were washed and incubated with claudin-5-FITC (green) and occludin-rhodamine (red)-specific antibodies. DAPI (blue) was used to stain the cell nuclei. Scale bar, 100 μm . (B) Quantification of (B) claudin-5 and (C) occludin intensity on the surface of HBECs was performed using NIH ImageJ software. Bars and error bars denote the means and SDs, respectively. Each symbol denotes a single cell measurement ($n = 10$ cells per group). Asterisks indicate P -value significance (* $P < 0.05$, ** $P < 0.01$ and **** $P < 0.0001$) calculated using one-way ANOVA and adjusted using the Tukey's post-hoc analysis. ns represents not statistically significant comparisons.

<https://doi.org/10.1371/journal.ppat.1010941.g004>

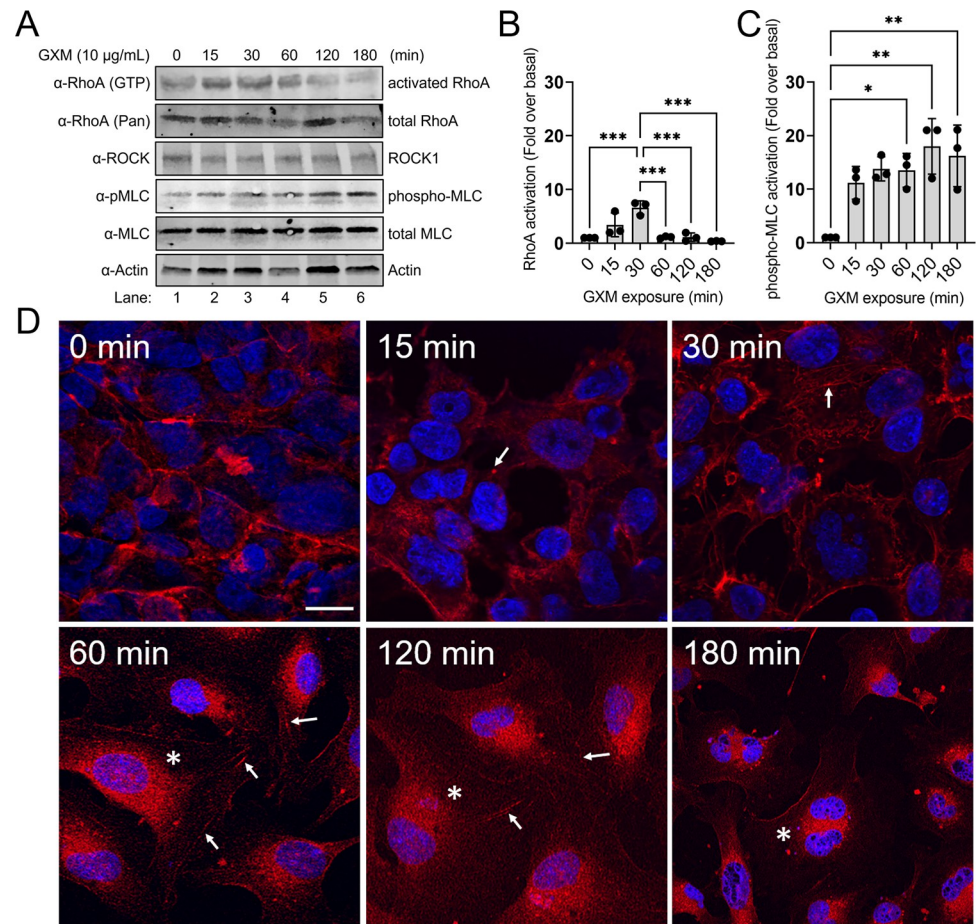


Fig 5. GXM augments the expression of activated RhoA and modulates the cytoskeleton in HBECs in a time-dependent manner. (A) WB analyses of HBEC lysates stimulated with 10 $\mu\text{g}/\text{mL}$ of GXM were performed to assess the expression of activated RhoA protein (GTP-bound) and phosphorylated myosin light chain (pMLC) over the course of 180 min. Quantitative measurements of individual band intensity in WB analyses described in panel A for (B) activated RhoA and (C) phospho-MLC using LiCOR Image Studio software. Bars represent the means of 3 independent gel results (black circles) and error bars indicate SDs. P -value significance (* $P < 0.05$, ** $P < 0.01$ and *** $P < 0.001$) was calculated using one-way ANOVA and adjusted using the Tukey's post-hoc analysis. (D) IF images of actin remodeling in HBECs after incubation in the absence (0 min) and the presence of 10 $\mu\text{g}/\text{mL}$ GXM for the indicated times (15–180 min). Cells were stained with Phalloidin-594 (red) and DAPI (blue). Arrows indicate actin stress fiber formation; asterisks represent perinuclear relocation of actin. Scale bar, 20 μm .

<https://doi.org/10.1371/journal.ppat.1010941.g005>

infection and development of cryptococcal meningoencephalitis (CME) [28]. To confirm that RhoA is activated during GXM-mediated disruption of TJ integrity, levels of both RhoA (pan) and RhoA-GTP (activated form) were measured in lysates of HBECs by WB analysis (Fig 5). HBECs ($n = 3$) were plated in 24-well plates and grown to confluency prior to stimulation with 10 $\mu\text{g}/\text{mL}$ of GXM over time (0, 15, 30, 60, 120, and 180 min; Fig 5A). RhoA activation was induced immediately upon stimulation by GXM, reaching a peak 6-fold increase after 30 min (Fig 5B). Interestingly, RhoA activation dropped to near-basal levels after 60 min before decreasing below basal levels at 180 min. RhoA activation is associated with increased cell permeability and actin cytoskeletal fiber formation [19], and its involvement in modulating TJ integrity is of interest during CME. RhoA signals through Rho-associated protein kinase (ROCK) to inhibit myosin-light chain (MLC) phosphatase [29] which in turn leads to stable phosphorylation and activation of MLC. Activated MLC mediates actin stress fiber formation

during endothelial barrier permeability [30]. We observed a 10-fold increase in MLC phosphorylation after 15 min of GXM stimulation, concurrent with activation of RhoA (Fig 5A and 5C). Interestingly, phosphorylation of MLC remained elevated after 120 min (Fig 5A and 5C), suggesting that actin remodeling is prolonged after initial RhoA stimulation. To assess the extent of actin remodeling in HBECs treated with GXM, we performed fluorescence confocal microscopy on cells stained with the fluorescent actin dye phalloidin and treated with GXM over time (0, 15, 30, 60, 120 and 180 min, Fig 5D). Although the levels of actin expression did not significantly change in response to GXM treatment (S3 Fig), we observed considerable change in the actin cytoskeleton following GXM stimulation. In untreated confluent HBEC monolayers (0 min), actin is localized to the periphery of cells (Fig 5D). Actin stress fibers (arrows) begin to form after 15 min of GXM stimulation and continue to develop over time. In addition, actin remodels away from the cell periphery to adopt a perinuclear localization (asterisks) after 60 min which persists throughout the rest of the experiment (Fig 5D). Disruption of the endothelial monolayer can be observed as early as 15 min, but is most prominent at 60, 120 and 180 min (Fig 5D). These results are consistent with the time course for MLC phosphorylation in response to GXM. Our data suggest that GXM-induced RhoA activation and RhoA-mediated actin cytoskeleton remodeling, may be mechanistically important for the paracellular crossing of *C. neoformans* as free yeast cells or inside of macrophages through the BBB during pathologic conditions.

GXM disrupts the trans-endothelial electrical resistance (TEER) of HBECs in a BBB model and enhances its permeability

The TEER is a widely accepted quantitative technique to measure the integrity of TJ dynamics in cell culture models of endothelial monolayers. Since GXM reduces the expression (*in vivo*) and distribution/intensity (*in vitro*) of TJs, we investigated the impact of the CPS on TEER of an *in vitro* BBB model that consisted of HBECs and pericytes (Fig 6A and 6B). Pericytes are cells present at intervals along the walls of blood vessels. In the CNS, they are important for blood vessel formation, maintenance of the BBB, regulation of immune cell entry to the CNS, and control of brain blood flow [31]. Currently, there is no data available on the role of pericytes in cerebral cryptococcosis. Hence, we investigated the advantage of having a single (HBECs) versus dual (HBECs + pericytes) *in vitro* BBB model (S4 Fig). The BBB model consisting of HBECs + pericytes demonstrated a significantly higher TEER (2-fold) than the system with only HBECs ($P < 0.01$), which suggest that pericytes substantially strengthen the interactions between HBECs. Using this model, all the BBBs treated with GXM or EDTA demonstrated a significant drop in TEER (~ 60% or more) 1 h post-exposure relative to the untreated and mock extract-treated BBBs ($P < 0.05$; Fig 6B). Mock extracts were prepared from acapsular *cap59* strain cells grown in cultures similarly to wild-type H99 to assure that GXM and not the traces from the reagents used in the procedure affect the permeability of the HBECs in the BBB model. EDTA-treated BBBs demonstrated a lower TEER percentage than BBBs incubated with 50 ($P < 0.05$) and 100 ($P < 0.01$) $\mu\text{g}/\text{mL}$ of GXM. Also, BBBs cultured with 100 $\mu\text{g}/\text{mL}$ of GXM exhibited lower TEER percentage than BBBs exposed to 10 $\mu\text{g}/\text{mL}$ of the fungal polysaccharide ($P < 0.01$). BBBs treated with 10 $\mu\text{g}/\text{mL}$ of GXM maintained ~ 60% TEER percentage reduction after 1 h compared to the control BBBs. Notably, all the other conditions demonstrated a 100% TEER or TJ integrity reduction in BBBs after 1 h. To better understand the minimal GXM concentration required for compromising the integrity of our *in vitro* BBB model, we performed a dose response curve exposing cells to 0.001 to 100 $\mu\text{g}/\text{mL}$ of GXM. (S5 Fig). We calculated that the inhibitory concentration (IC_{50}) needed to make the system 50% permeable was 9.95 $\mu\text{g}/\text{mL}$ of GXM. The mock extract treatment had no effect on

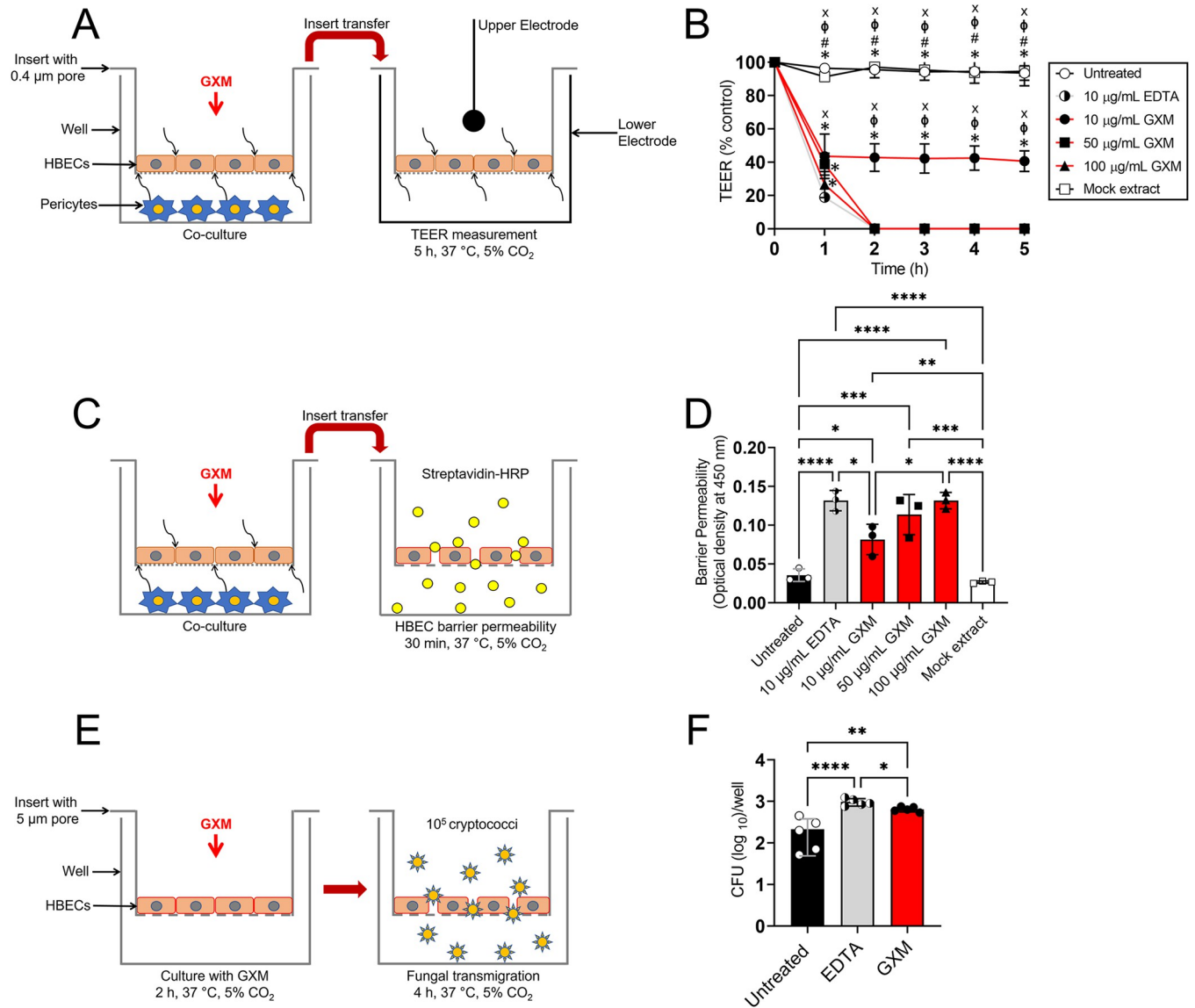


Fig 6. GXM decreases the trans-endothelial electrical resistance (TEER) and transmigration of *C. neoformans* through HBECs in a blood brain barrier (BBB) model. Graphic representation of the HBECs and pericytes BBB model used for the (A) TEER measurements, (C) HBEC barrier permeability assay, and HBEC model used for the (E) fungal transmigration assay. For A and C, HBECs and pericytes were grown separately (HBECs, 0.4 µm pore insert; pericytes, bottom of a well) and co-incubated using a microtiter transwell system that permits chemotactic exchange through the supernatant. (B) Relative TEER of HBECs incubated with GXM (10, 50, or 100 µg/mL) for 5 h at 37°C and 5% CO₂. HBECs incubated alone (negative), with EDTA (10 µg/mL; positive), or with mock extract from acapsular strain *cap59* (negative) were used as controls. Time points are the averages of the results for three different TEER measurements, and error bars denote SDs. Symbols (*, #, φ, and x) indicate *P* value significance (*P* < 0.05) calculated using one-way ANOVA and adjusted using the Tukey's post-hoc analysis. *, #, φ, and x indicate significantly higher TEER than in the 10 µg/mL of EDTA-, 10 µg/mL of GXM-, 50 µg/mL of GXM-, and 100 µg/mL of GXM-treated groups, respectively. (D) Relative HBEC barrier permeability to streptavidin-horseradish peroxidase (HRP) after incubation with GXM (10, 50, or 100 µg/mL) for 30 min at 37°C and 5% CO₂. HBECs incubated alone (negative), with EDTA (10 µg/mL; positive), or with mock extract (negative) were used as controls. (E) HBECs were cultured for 2 h with 10 µg/mL of GXM in a microtiter transwell system (5 µm pore insert). Then, 10⁵ cryptococci were added to the well and fungal transmigration through the HBECs was determined for 4 h using CFU. (F) CFU determinations after fungal transmigration are shown. HBECs incubated alone or with EDTA (10 µg/mL) were used as negative and positive controls, respectively. For B, D, and F, bars and error bars denote the means and SDs, respectively. Each symbol denotes a single well measurement (*n* = 3 wells per group for B and D) or CFU determinations from a single well (*n* = 5 wells per group for F). Asterisks indicate *P*-value significance (* *P* < 0.05, ** *P* < 0.01, *** *P* < 0.001 and **** *P* < 0.0001) calculated using one-way ANOVA and adjusted using the Tukey's post-hoc analysis. These experiments were performed thrice, similar results were obtained each time, and all the results combined are presented.

<https://doi.org/10.1371/journal.ppat.1010941.g006>

the integrity of the *in vitro* BBB (S5 Fig). Then, we assessed the BBB permeability to streptavidin-horseradish peroxidase (HRP) after 1 h treatment with GXM or EDTA (Fig 6C and 6D). All the GXM (10 $\mu\text{g}/\text{mL}$, $P < 0.05$; 50 $\mu\text{g}/\text{mL}$, $P < 0.01$; 100 $\mu\text{g}/\text{mL}$, $P < 0.001$)- or EDTA ($P < 0.001$)-treated HBECs exhibited significantly more permeability than the untreated and mock extract-treated cells (Fig 6D). HBECs cultured with concentrations $\geq 50 \mu\text{g}/\text{mL}$ of GXM or 10 $\mu\text{g}/\text{mL}$ of EDTA displayed similar increased in barrier permeability to streptavidin-HRP. HBECs incubated with 10 $\mu\text{g}/\text{mL}$ of GXM demonstrated considerably lower barrier permeability than EDTA-treated ($P < 0.05$) cells, respectively. Our experiments demonstrated that GXM disturbs the TEER and integrity of HBEC-closed interactions in a BBB *in vitro* model.

Given that GXM inhibits the expression of TJs and alters the TEER in HBECs, we investigated the permeability of HBECs to *C. neoformans* strain H99 cell transmigration after pre-incubation with 10 $\mu\text{g}/\text{mL}$ of GXM or EDTA for 1 h (Fig 6E). GXM- ($P < 0.01$) and EDTA- ($P < 0.0001$) treated HBECs demonstrated significant passage of cryptococci compared to untreated cells (Fig 6F). EDTA had the highest cryptococcal BBB transmigration, followed by GXM and untreated HBECs, respectively. Our studies indicate that GXM promotes HBEC disruption and *C. neoformans* penetration.

GXM stimulates vasodilation of blood vessels via endothelium-dependent mechanisms

To understand the influence of *C. neoformans* GXM on endothelial cells of blood vessels, mouse superior mesenteric arteries (SMA) were isolated, cultured in absence or presence of 25 $\mu\text{g}/\text{mL}$ of GXM *ex vivo* for 40 min, and evaluated for vascular reactivity using a wire myograph in presence of acetylcholine (ACh; to test for endothelium-dependent vasodilation) and phenylephrine (PE; to test for vasoconstriction) (Fig 7). Despite the selected concentration of 25 $\mu\text{g}/\text{mL}$ of GXM for this *ex vivo* assay could be in the high physiological end of the infection spectrum in serum, animal-to-animal variations, although rare, has been reported with a mouse reaching the hundreds of $\mu\text{g}/\text{mL}$ [25]. SMA incubated with the CPS were less responsive to PE and decreased their contraction relative to untreated arteries ($n = 5$ per group;

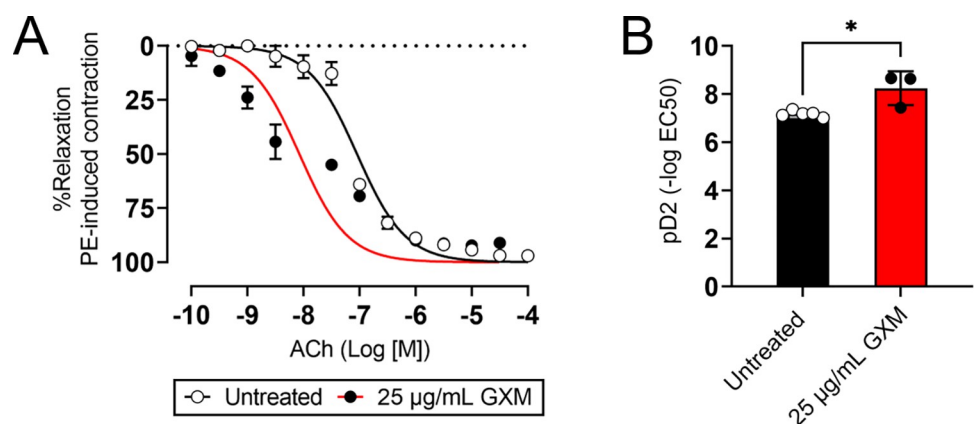


Fig 7. GXM causes vasodilation of mouse blood vessels after *ex vivo* treatment. (A) Murine superior mesenteric arteries (SMA) incubated in absence (untreated) or presence of 25 $\mu\text{g}/\text{mL}$ GXM were evaluated in response to phenylephrine (PE; test for vasoconstriction) or acetylcholine (ACh; test for endothelium-dependent vasodilation). Cumulative concentration-response curves are shown. Each point represents the average of 5 individual SMA measurements. The concentration-response curve was log-transformed, normalized to percent maximal response, and fitted using a nonlinear regression. P values of < 0.05 were considered significant. (B) pD_2 for ACh curve. Each symbol ($n = 5$, untreated; $n = 3$, GXM-treated SMA rings) represents a single SMA ring. Bars and error bars denote the mean value and SDs, respectively. Asterisk denotes P -value significance ($* P < 0.05$) calculated using student's t -test analysis.

<https://doi.org/10.1371/journal.ppat.1010941.g007>

Fig 7A). However, arteries incubated with 25 $\mu\text{g}/\text{mL}$ of GXM were substantially more sensitive to ACh and significantly increased their vasodilation compared to untreated blood vessels (Fig 7A). We corroborated that GXM-treated SMA ($n = 3$) were significantly more sensitive to ACh than untreated arteries ($n = 5$; $P < 0.05$; Fig 7B). We concluded that GXM promotes blood vessel relaxation by endothelium-dependent mechanisms, providing proof of principle evidence that the cryptococcal CPS alters the integrity of the vasculature, enabling systemic dissemination from the respiratory system to the CNS.

Discussion

C. neoformans capsular GXM is released into tissues during infection where it accumulates and causes a range of adverse immunological effects [17]. Individuals with CME frequently suffer from the detrimental effects associated with increased intracranial pressure such as edema, hydrocephalus, and subarachnoid space hemorrhage, which may be related in part to GXM-mediated effects [32]. The concentration of GXM in CSF can reach 1 mg/mL [33] and post-mortem pathological examinations of brains from patients with CME indicate that this polysaccharide is extensively deposited in tissue [17]. We evaluated the role of exogenous GXM on the development of *C. neoformans* pulmonary infection by i.n. challenging C57BL/6 mice. However, we first determined the extent of exogenous GXM dissemination post-inoculation using ELISA. GXM was detected in lung and serum in comparable concentrations to other similar studies in rodents [14,34]. Exogenous GXM i.n. challenge of mice prior infection results in lung inflammation, although whether the response exacerbates pulmonary cryptococcal colonization and/or dissemination to the CNS via single cell escape or using the Trojan horse mechanism require further investigation. For example, it is conceivable that GXM impairs the intercellular junctions in the epithelial cells of the lungs allowing the escape of individual cryptococci and/or inside of macrophages. While *C. neoformans* capsular GXM is cleared from the bloodstream within days, it can be retained in organ tissues for weeks, especially those of the liver and spleen [35]. Surprisingly, we also detected low levels of GXM in brain tissue, validating that this delivery was appropriate to study the impact of the CPS on the development of cryptococcosis. It is also important to point out that the concentrations of GXM used in our studies are not out of context or in the high-end of the spectrum. CPS concentrations ranging from 50–800 $\mu\text{g}/\text{mL}$ have been extensively used in the field of cryptococcosis to understand the role of this fungal antigen on the host immune or specifically Ab responses [14,21,25,34]. In our study, we are using similar tools (e.g., exogenous GXM administration, mouse model, Abs, etc.) as previously described and adding innovative *in vitro* and *ex vivo* techniques to understand how *C. neoformans* crosses the BBB. To provide a typical i.t. infection baseline, we measured the GXM levels of the lungs, serum, and brain after pulmonary infection with *C. neoformans* strain H99 without GXM pre-conditioning. GXM accumulation in tissues and serum during a typical i.t. infection is comparable to previous reports in the field of cryptococcosis [14,25,26].

We investigated the impact of exogenous GXM on the development of *C. neoformans* infection and demonstrated that CPS accelerates cryptococcosis in C57BL/6 mice. Pulmonary cryptococcal infection of GXM-challenged rodents was characterized by substantial colonization of the epithelial tissue, extensive CPS accumulation surrounding cryptococci in a biofilm-like arrangement, and minimal inflammation. It is possible that prior priming of the respiratory tissue with GXM to cryptococcal infection enhances the ability of the fungus to adhere and colonize the airway epithelium. Although *cap67*, a strain with defective capsular production, has shown higher adhesion to human epithelial-like cells than clinical encapsulated strains [36], phospholipase B [37], mannoprotein MP84 [38], and heat-shock protein 70 [39] have been

shown to influence the attachment of *C. neoformans* to pulmonary-like cells. i.n. challenge of mice with GXM may even create a competitive advantage over other possible ligands involved in the association of the carbohydrate with surface receptors on epithelial cells [39]. Moreover, active production and release of CPS by *C. neoformans* are required for biofilm formation [40], which involves a robust attachment to the surface substrate. Substantial accumulation of CPS around cryptococci in GXM-sensitized animals demonstrates a biofilm-like structure in lung tissue that prevents antifungal immune responses such as cellular migration, phagocytosis, and clearance, providing evidence for the involvement of GXM in the progression of *C. neoformans* invasion.

Given that *C. neoformans* infection was more difficult to control in the lungs of GXM-challenged mice, these animals also evinced higher hematogenous fungal load than the untreated rodents. It is conceivable that the slight immune response mediated the collapse of the lung tissue and vasodilation of the blood vessels, allowing substantial cryptococcal cell proliferation and extensive production/release of the CPS [41]. In this regard, portions (M2 motif) of the *C. neoformans* capsular GXM have been shown to elicit non-protective Abs, which may affect phagocytic cell responses in the lungs and result in the inability of the host to control the infection [42]. Mice lacking claudin-18, a TJ protein highly expressed in airway tissues, exhibited increased susceptibility to *C. deneoformans* infection through massive multiplication of yeast cells with poor granulomatous responses, reduced production of interferon- γ , and acidification of the alveolar space despite increased presence of immune cells such as CD4⁺ T cells [43]. In addition, GXM has detrimental effects on endothelial cells associated with blood vessels including alterations of adhesion molecules important for the migration of leukocytes to fight off the infection [44,45] and vascular vasodilation [46] following cryptococcal infection, which increases vessel tension and promotes fungal dissemination [46]. Untreated mice i.t.-infected with *C. neoformans* H99 demonstrated similar blood load to those reported by others [47–49]. However, it is unclear why these mice evinced a reduction in the lung fungal burden as the infection progressed from 3- to 7-dpi. A plausible explanation may be dissemination of cryptococci to other organs (e.g., liver, spleen, kidneys, etc.) not necessarily accounted for or analyzed in these studies. This possibility is conceivable since higher cryptococcal burden was detected 7-dpi in blood and the fact that not all the untreated mice die in the survival experiment 30-dpi.

GXM sensitization prior to infection increased *C. neoformans* load in the CNS. There was approximately a 3-fold CFU count difference between brains excised from untreated and GXM-challenged mice 7-dpi. Since the exogenous GXM was administered to the animals i.n., this capsular component deposited mostly in the lungs and reached serum in low levels as similarly described in [14]. Even though GXM injection into the bloodstream does not reach to the CNS due to the unidirectional movement of the CPS across the BBB from the CSF to serum [34,50], the ELISA and IF data produced in this investigation demonstrated that i.n. delivery of GXM reaches the CNS likely through the nasal cavity. A recent study showed that i.n. *C. neoformans* infection was found in the upper respiratory tract and fungal brain invasion occurred quickly in ≤ 3 h [51]. GXM-treated mice showed higher number of cryptococcomas and larger cryptococcal brain lesions than those found in untreated brains. Likewise, GXM localized in blood vessels in brain parenchyma, and its deposition may have serious implications in the maintenance of the host BBB integrity. Vascular GXM accumulation and fungal occlusion have been described by others [52,53] and validated by us [32] as responsible of infarction and hemorrhagic dissemination in CME patients and animal models [46], respectively. Notably, the cortex and hippocampus of GXM-challenged mice were the most affected regions of the brain, suggesting that these animals may also show behavioral and cognitive impairment. In fact, altered mental status in HIV⁺ patients with CME is associated with high

mortality rates [54,55]. It is possible that GXM acts as a chelator and binds to metal ions (e.g., Ca^{2+}) contributing to its detrimental effects in the BBB and/or cells of the brain. Although these provocative thoughts are outside of the scope of this study, future investigations are needed to understand the impact of cryptococcal infection and GXM on behavior and cognition.

We found that i.n. GXM instillation (concentrations: 15.6–125 $\mu\text{g}/\text{mL}$) alone disrupted TJ and adhesion proteins in rodents, validating the importance of this polysaccharide in destabilizing the BBB and promoting traversal passage of *C. neoformans* into the CNS. TJ and adhesion proteins are important in the molecular architecture of the cell and *C. neoformans* interactions with BBB endothelial cells mediate alterations in the cytoskeleton of the mammalian cells [56]. GXM has been shown to have a profound impact on HBEC TJs. Claudin-5, ZO-1, and JAM-A were downregulated at concentrations $\geq 62.5 \mu\text{g}/\text{mL}$, whereas occludin seemed to be more susceptible to GXM and was reduced at concentrations $\geq 15.6 \mu\text{g}/\text{mL}$. WB analyses in murine brain extracts 24 h after GXM sensitization and IF in HBECs cultured with the CPS for 4 h demonstrated a significant reduction in the expression/distribution of claudin-5 and occludin. These integral proteins are located in the apical region of the cell and act as gatekeepers for BBB paracellular passage. Our results are consistent with Chen and colleagues, who demonstrated that occludin dysregulation is associated with weakened endothelial cell interactions in the BBB [56]. Moreover, the *in vivo* GXM sensitization studies showed that the expression of actin, a housekeeping protein that form microfilaments in the cytoskeleton and have intimate interactions with cellular membranes, is affected. We suspect that GXM binds to actin altering its expression and causing very important structural modification to the cytoskeleton in endothelial cells, therefore, having a critical impact in *C. neoformans* BBB penetration. It is possible that these GXM-driven modifications to the cytoskeleton may explain the susceptibility of endothelial cells in the BBB interface to allow both cryptococcal transcellular and/or paracellular passage of single cells or cells inside of phagocytes to the brain parenchyma. However, further studies need to be performed and other virulence factors need to be considered. To rule out the possibility that GXM instillation may damage BBB's endothelial cells in mice due to high concentration overload, we have tested GXM instillation in mice up to 500 $\mu\text{g}/\text{mL}$ and TJ expression increases at that concentration suggesting TJ expression can be recovered. The same pattern is observed in the actin bands. Interestingly, we have observed a similar pattern associated with normal cryptococcosis (no GXM instillation) progression, which indicates that the inhibition of intercellular junctions and actin is transient and can be reverted especially upon cryptococci invades and colonize the CNS.

It is also significant to mention that TJs impact structural changes in the cell that can be important in the transcellular passage of free cells, as well as those being transported inside of macrophages. Our findings of GXM-induced RhoA activation substantiates the impact of this CPS on the BBB structural integrity during *C. neoformans* invasion. Although the involvement of RhoGTPases in the translocation of *C. neoformans* from the blood capillaries to the brain parenchyma has been previously suggested [28], we demonstrated that GXM may regulate fungal transmigration by causing rapid structural changes in the BBB including weakening of TJ and disruption of HBEC interactions (Fig 8). GXM stimulates activation of RhoA, which activates ROCK [56]. ROCK inhibits the myosin-light chain (MLC) phosphatase, leading to actin stress fiber formation through enhancement of MLC phosphorylation [57]. Actin stress fibers contribute to the internalization and lysosomal degradation of claudin and occludin, disrupting TJs between brain microvascular endothelial cells [58]. These observations are significant because further studies can focus on strengthening TJ interactions between neighboring HBECs in individuals with pulmonary cryptococcosis and help the development of novel strategies to prevent CME and its associated morbidity. Furthermore, investigating the role of

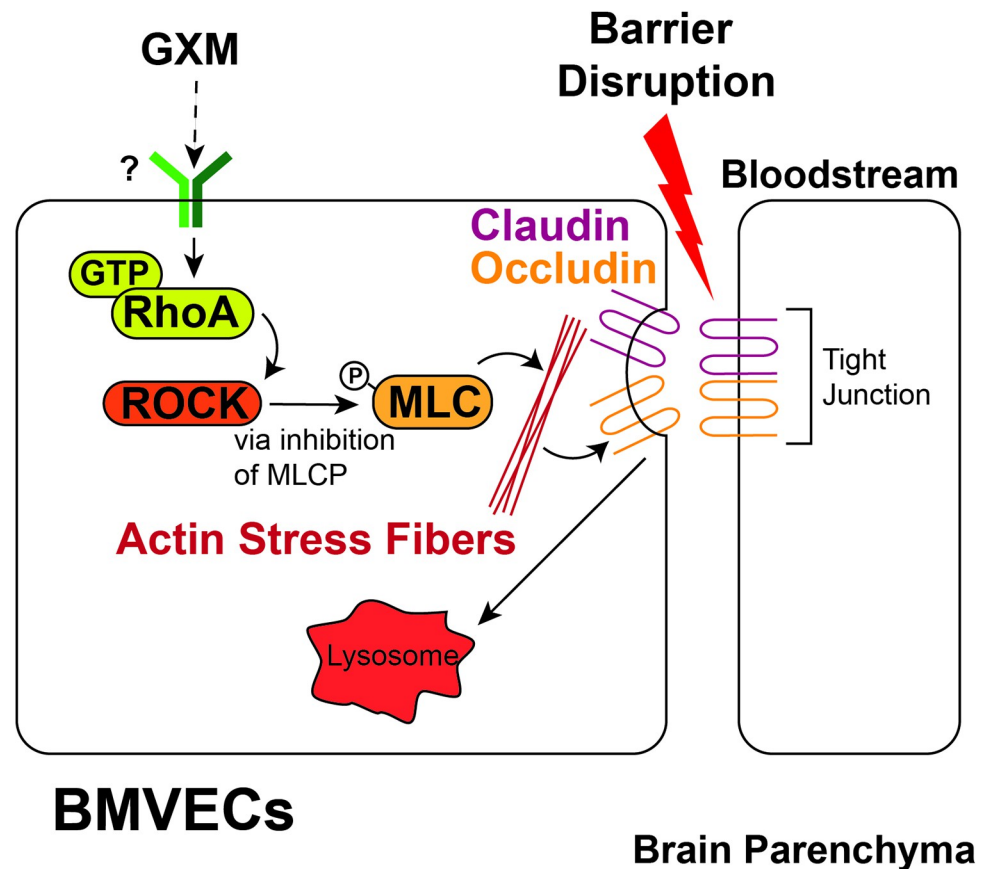


Fig 8. Model of GXM-mediated disruption of the BBB during cryptococcal infection. GXM stimulates activation of RhoA, which activates Rho-associated protein kinase (ROCK). ROCK inhibits the myosin light chain phosphatase (MLCP), leading to actin stress fiber formation through enhancement of MLC phosphorylation. Actin stress fibers contribute to the internalization and lysosomal degradation of claudin and occludin, disrupting TJs between brain microvascular endothelial cells (BMVECs).

<https://doi.org/10.1371/journal.ppat.1010941.g008>

GXM as a modulator of TJ and BBB integrity may be of interest for future studies. For instance, the receptor on the surface of HBECs that recognizes GXM and triggers the RhoA signaling pathway still needs to be identified.

Due to the difficult nature of investigating the interaction of *C. neoformans* with the neurovascular unit *in vivo*, the use of microtiter transwell systems to mimic the BBB has proliferated in the past two decades [8,56,59–63]. Since we demonstrated that GXM alters the distribution of TJs on HBECs, we assessed the impact of GXM on the TEER of HBEC monolayers grown in transwells and co-incubated with pericytes separated by a membrane that allows the exchange of secreted factors by the cells in co-culture. GXM quickly reduced the TEER across the HBEC monolayer in presence of pericytes, suggesting disruptions in TJs and the integrity of the HBEC neighboring interactions. Little is known on the role of pericytes on *C. neoformans* BBB transmigration *in vivo*. However, a deficiency of pericytes in the CNS can cause increased BBB permeability due to their ability to cover endothelial cells that line the capillaries [64]. Our findings demonstrated that the BBB model consisting of HBECs and pericytes had a 2-fold TEER measurement compared to the system with only HBECs, suggesting that pericytes markedly reinforce the BBB integrity. This important observation warrants future studies on the importance of pericytes in *C. neoformans* and BBB interactions. Also, our studies highlight

the importance of having critical consideration in the design of *in vitro* models that mimic the BBB, particularly to investigate microbial CNS invasion. Studies to elucidate the basic functions of pericytes in *C. neoformans* transmigration require such pericyte-endothelial cell communication for a more comprehensive understanding of cerebral cryptococcosis.

We demonstrated GXM-treated HBECs grown in transwells displayed higher permeability and passage to cryptococci relative to the untreated and EDTA-treated HBEC conditions. It is plausible that both transmigration processes, trans- and para-cytosis, occurred in this *in vitro* system. GXM exposure to HBECs resulted in a significant reduction of TJ distribution on their surface and decreased TEER, indicating that fungal crossing between endothelial cells was taking place. We did not examine HBEC transcellular passage, but this mechanism of BBB penetration and CNS invasion has been extensively described in free cryptococci [8,56] and cryptococci trolleying inside phagocytic cells [60]. Though the specific mechanism of *C. neoformans* brain invasion involved in this process is not yet confirmed, it may be sensible to embrace the idea that all the transmigration processes described, including the Trojan horse, simultaneously and dynamically occur during infection.

Surprisingly, GXM addition to the *in vitro* BBB model caused a dramatic reduction in the BBB integrity and TEER, which can be explained by our finding of 9.95 $\mu\text{g}/\text{mL}$ of GXM as the minimal concentration required for compromising the barrier integrity. In contrast, there was no defect when adding cryptococci, which also produce and shed GXM in the medium. It is necessary to distinguish that BBB permeability is not synonymous of fungal transmigration which may explain the differences observed between the dramatic reduction of TEER and the marginal although still statistically significant variations observed between the different conditions (e.g., untreated, EDTA, and GXM) in the *C. neoformans* transmigration assay. It also must be considered how difficult is for microbes to cross the BBB, which in addition to battling with immune cells and their mediators in the bloodstream, need to deal with the steric hindrance of the barrier to penetrate the brain parenchyma. Although cryptococci certainly cross the BBB *in vitro*, the low efficiency of the phenomenon [65] is also a challenge for interpretation of the findings and their translation into *in vivo* or clinical situation.

In conclusion, we demonstrated that exogenous GXM administration exacerbates lung colonization, systemic dissemination, and CNS invasion. GXM has detrimental defects on TJs facilitating its translocation from the lungs to the CNS suggesting the importance of developing therapeutics to strengthen cell-to-cell interactions, particularly in the early stages of the disease. Our findings have significant implications in understanding the different mechanisms used by the fungus to cross the BBB and colonize the brain resulting in its main manifestation, CME, which has high mortality. Additional investigations are necessary to establish the molecular mechanisms by which GXM impairs TJ function and impacts cryptococcal systemic disease.

Materials and methods

Ethics statement

All animal studies were conducted according to the experimental practices and standards approved by the Institutional Animal Care and Use Committees at the New York Institute of Technology College of Osteopathic Medicine (Protocol #: 2016-LRM-01). This study was carried out in compliance with the Animals in Research: Reporting *In vivo* Experiments guidelines [66].

C. neoformans

C. neoformans strain H99 (serotype A) was isolated and kindly provided by John Perfect at Duke University. *cap59* is an acapsular mutant strain derived from H99 by Joseph Heitman at

Duke University and this gene functions in GXM export [67]. Yeast cells were grown in Sabouraud dextrose broth (pH 5.6; BD Difco) for 24 h at 30°C in an orbital shaker (Thermo Fisher; TF) set at 150 rpm (to early stationary phase).

GXM isolation

GXM was isolated from *C. neoformans* strain H99 using the hexadecyltrimethyl ammonium bromide (CTAB) method as previously described [68] with a few modifications. *C. neoformans* strain *cap59* was used to perform a mock extraction. Briefly, fungal cells (10^9) were inoculated into 1,000-mL Erlenmeyer flasks containing 400 mL of minimal medium composed of glucose (15 mM), MgSO_4 (10 mM), KH_2PO_4 (29.4 mM), glycine (13 mM), and thiamine-HCl (3 μM), pH 5.5. Fungal cells were cultivated for 3 days at 30°C with shaking and separated from culture supernatants by centrifugation at 4,000 x g (15 min, 4°C). The supernatant fluids were collected and centrifuged again at 15,000 x g (15 min, 4°C) to remove smaller debris. The pellets were discarded, and the resulting supernatant was concentrated approximately 20-fold using an Amicon (Millipore) ultrafiltration cell (with a cutoff of 100 kDa and a total capacity of 200 mL) with stirring and Biomax polyethersulfone ultrafiltration discs (63.5 mm). A nitrogen (N_2) stream was used as the pressure gas. After the supernatant was concentrated, a thick, translucent film was observed in close association with the ultrafiltration disc and was covered by a concentrated fluid phase. The fluid phase was discarded, and the viscous layer was collected with a cell scraper for storage at room temperature (RT). Fractions that were passed through the 100-kDa filtration discs were filtered through 10-kDa membranes, resulting again in film formation. We heat inactivated (100°C for 15 min) proteases in our GXM preparation. Additionally, each preparation was treated with protease inhibitor cocktail (37°C for 2 h). Each preparation was also tested for contamination with bacterial lipopolysaccharide (LPS) using the Limulus amoebocyte lysate (LAL) assay (Lonza). LPS was undetected in the LAL assay. We performed CFU determinations in our preparations and did not observe any culturable microbial growth. For polysaccharide quantification, a capture ELISA [69], the carbazole reaction for hexuronic acid [70], and the method for hexose detection described by Dubois et al. [71] were used.

In vivo GXM sensitization and pulmonary model of *C. neoformans* infection

Male and female C57BL/6 mice (10–12 weeks old; Charles Rivers) were anesthetized using the ketamine (100 mg/kg)-xylazine (10 mg/kg) cocktail (Covetrus) and i.n. challenged with a 50 μL solution of PBS (untreated) or GXM (125 $\mu\text{g}/\text{mL}$) in PBS 24 h prior to cryptococcal pulmonary infection. Then, animals were anesthetized using the ketamine-xylazine cocktail and a vertical 5-mm incision was made in the skin of the ventral neck just right of midline. The trachea was identified and injected with a 100 μL suspension containing 10^5 *C. neoformans* strain H99 yeast cells using a 26-gauge syringe. The anterior neck site was closed with surgical glue and 1% topical chlorhexidine solution was applied over the closed incision. A group of mice was monitored for survival studies. A separate group of GXM challenged/infected mice were bled from the facial vein (0.1 mL blood collected), euthanized in a chamber with 30–70% CO_2 flow, and brain/lungs excised for CFU count determinations and histological processing.

Determination of GXM levels

C. neoformans capsular GXM in organs and serum were measured by capture ELISA as described [72] and modified accordingly for this study. Organ tissue (0.2 g) was placed in 2 mL of PBS, homogenized, and the supernatant stored at -20°C until quantified. Briefly,

microtiter polystyrene plates were coated with goat anti-mouse (GAM) IgM (1 µg/mL) and blocked with 1% bovine serum albumin (BSA) in PBS. Next, the IgM GXM binding mAb 2D10 (2 µg/mL) was added as a capture Ab [73], and the plate was incubated for 1 h. Culture supernatants were serially diluted on the plate and incubated for 1 h. The ELISA was completed by adding, in successive steps, mAb 18B7 (2 µg/mL) in buffer (PBS with 1% BSA), 1 µg of alkaline phosphatase-labeled GAM IgG1/mL in buffer, and 50 µl of *p*-nitrophenyl phosphate (5 mg/mL) in substrate buffer (0.001 M MgCl₂ and 0.05 M Na₂CO₃, in 1 L [pH 9.8]). Between each step, the wells were washed with 0.05% Tween 20 in tris-buffered saline (TBST). All incubations were done at 37°C for 1 h or 4°C overnight.

CFU determinations

Lung and brain tissues were excised from euthanized mice 3- and 7-dpi. The right lobe of lung and the right hemisphere of the brain were homogenized in 5 mL of sterile PBS, serially diluted, a 100 µL suspension was plated on Sabouraud dextrose agar (BD Difco) and incubated at 30°C for 48 h. Quantification of viable yeast cells from untreated and GXM-challenged animals were determined by CFU counting.

Histological examinations

a. Lungs. Lung tissue was excised from euthanized mice 7-dpi and fixed in 10% formalin for 24 h, processed, and embedded in paraffin. Four-micrometer vertical sections were cut and then fixed to glass slides and subjected either to H&E stain or to mucin carmine stain, to examine host tissue and fungal morphology, respectively. Microscopic examinations of tissues were performed sequentially by light microscopy with a Leica DMi8 inverted microscope (20 and 40X objectives), and photographed with a Leica DFC7000 T digital camera using the Leica software platform LAS X. Multiple slides were visualized and examined to understand host tissue inflammation and fungal distribution.

b. Brain. *C. neoformans* cells and CPS released in tissue were stained using GXM-specific mAb 18B7. Slides were blocked, and mAb 18B7 (2 µg/ml) was added for 1 h at 37°C. After the slides were washed, fluorescein isothiocyanate (FITC)-conjugated GAM Ab [dilution, 1:250; 1% BSA] was applied for 1 h at RT. Neurons in tissue sections were stained with DAPI (4',6-diamidino-2-phenylindole) and microtubule-associated protein-2 (MAP-2) as described previously [74]. Microscopic examinations of brain sections were performed with a fully motorized Carl Zeiss Axio Observer Z1 confocal microscope. Confocal images of blue, green, and red fluorescence were conceived simultaneously using a multichannel mode. Z-stack images and measurements were corrected utilizing Zen software in deconvolution mode.

WB analysis of mouse brain cells

WB analysis was conducted using cytoplasmic extracts from mouse brain cells made with a NE-PER nuclear and cytoplasmic extraction kit (TF). The mixture was centrifuged at 10,000 × g for 10 min at 4°C, and the resulting protein content of the supernatant was determined using the Bradford method, employing a Pierce BCA protein assay kit (TF). Lysates were preserved in a protease inhibitor cocktail (TF) and stored at –20°C until use. Extracts were diluted with 2 × Laemmli sample buffer (Bio-Rad) and β-mercaptoethanol (Sigma). The mixture was heated to 90°C for 5 min. Twenty-three µg of protein were applied to each lane of a gradient gel (7.5%; Bio-Rad). Proteins were separated by electrophoresis at a constant 130 V/gel for 90 min and transferred to a nitrocellulose membrane on the Trans-Blot Turbo Transfer System (Bio-Rad) at 25 V for 7 min. The membranes were blocked with 5% BSA in TBST (0.1% Tween 20) for 2 h at RT. A primary claudin-5-, ZO-1-, occludin-, or JAM-A-specific mAb

(dilutions, 1:1000; Santa Cruz Biotechnology) was incubated overnight at 4°C with TBST (5% BSA). After washing the membranes 3X with TBST for 10 min, a GAM IgG (H + L) conjugated to HRP was used as a secondary Ab (dilution, 1:1000; Southern Biotech) and incubated with TBST (5% BSA) for 1 h at RT. The membranes were washed as described above. Protein bands were measured using the UVP ChemStudio imaging system (Analytik Jena) after staining each membrane with chemiluminescence detection reagents (TF). Quantitative measurements of individual band intensities in WB analyses for claudin-5, ZO-1, occludin, or JAM-A were performed using the NIH ImageJ software. Actin (dilution, 1:1,000; BD Biosciences), a cytoskeleton housekeeping protein, was used as loading controls to determine the relative intensity ratio. This WB protocol was previously described in [75] and modified accordingly for this study.

WB analysis of HBEC signaling assay

Whole cell lysate was collected from Human Brain Endothelial Cells-5i (HBECs, American Type Culture Collection [ATCC]) grown in 24-well tissue culture dishes in 2x Laemmli Sample Buffer. Samples were incubated for 5 min at 95°C to denature proteins and then loaded onto 4%-20% gradient SDS-PAGE gels (BioRad). Proteins were transferred to nitrocellulose blotted with RhoA-GTP (New East Biosciences), RhoA (Pan) ROCK, phosphor-MLC, and MLC (Cell Signaling Technologies) mAbs diluted (1:1000) in 1x TBST (1% BSA). WBs were then incubated with GAM 680 and GA-rabbit 800 (LiCOR Biosciences) secondary Abs. Revert 520 Total protein stain (LiCOR) was used for WB normalization. Blot images were collected using an Odyssey FC imager (LiCOR) and protein levels were quantified using LiCOR Image Studio software.

IF confocal microscopy

HBECs were seeded at 0.75×10^5 cells/glass coverslips in 24-well tissue culture plates and cultured for 24 h at 37°C and 5% CO₂. Then, monolayers of cells were incubated without or with 10 µg/mL of GXM for 4 h at 37°C and 5% CO₂. EDTA (10 µg/mL; Sigma) was used as a positive control. After each incubation, the solution with either GXM or EDTA was removed, and each coverslip fixed in a 4% paraformaldehyde solution for 10 min. Then, HBECs were rinsed 3X with PBS and blocked with PBS supplemented with 1% BSA followed by the addition of claudin-5-conjugated FITC and occludin-conjugated rhodamine binding mAbs (dilutions, 1:1000) in 1% BSA. Actin was stained with alexa-fluor phalloidin-594 (dilution, 1:500; Thermo Scientific). The plate was then incubated for 1 h at 37°C. DAPI was diluted in PBS and used to stain HBEC nuclei for 1 h at RT. Slides were examined by confocal microscopy as described above and analyzed using NIH ImageJ software. Individual cells in each IF image were traced, the intensity of each protein determined, and the mean intensity per condition reported.

BBB model

HBECs were seeded at 0.75×10^5 cells/well in 0.4 µm pore transwells (Greiner Bio-ONE) and grown at 37°C. Concurrently, human primary pericytes (Sciencell) were seeded at 1.5×10^5 cells/well in 24-well tissue culture plates. After 24 h, transwells containing HBECs were transferred to wells containing pericytes and grown for 48 h.

a. Trans-Endothelial Electrical Resistance. Relative TEER of HBECs incubated with GXM (10, 50, or 100 µg/mL) for 5 h at 37°C and 5% CO₂ was recorded. HBECs incubated alone (negative), with EDTA (10 µg/mL; positive), or with mock extract (negative) were used as controls. TEER was performed for 5 h using a CellZScope-E (nanoAnalytics). Fig 6A illustrates the HBECs and pericytes BBB model used for the TEER measurements.

b. Streptavidin-HRP HBEC Barrier Permeability. Cells were stimulated with GXM for 1 h. Permeability of barriers was assayed by adding streptavidin-HRP (BD Biosciences) to the upper chamber and collecting samples from the bottom chamber after 30 min incubation at 37°C and 5% CO₂. Samples were treated with 3,3',5,5' tetramethylbenzidine (Sigma) and quenched with 2 M H₂PO₄ in a 96-well plate. Absorbance was measured at 450 nm, as described previously [76]. Fig 6C depicts the BBB model used for the endothelial cell barrier permeability assays.

Fungal transmigration studies

The *in vitro* BBB model consists of primary HBECs seeded at a density of 10⁵ in 5 μm pore transwells and grown for 24 h at 37°C, 5% CO₂. Then, we analyzed the passage of *C. neoformans* (10⁵ cryptococci) through the BBB *in vitro* for 4 h to determine the impact of GXM (10 μg/mL) on the integrity of the barrier. Untreated or EDTA (10 μg/mL)-treated tissue constructs were used as controls. CFU determinations after fungal transmigration were performed. Fig 6E shows the HBECs BBB model used for the cryptococcal transmigration determination.

Vascular reactivity to GXM

Isolated superior mesenteric arteries (SMA) were incubated in oxygenated Krebs buffer (130 mM NaCl, 14.9 mM NaHCO₃, 4.7 mM KCl, 1.18 mM KH₂PO₄, 1.17 mM MgSO₄-7H₂O, 1.56 mM CaCl₂-2H₂O, 0.026 mM EDTA, 5.5 mM glucose, pH 7.4), with the perivascular fat carefully removed. SMA were cut into rings (2 mm in length) and cultured in vascular medium (ATCC) in an incubator at 37°C supplied by 5% CO₂. SMA were treated *ex vivo* with 25 μg/mL of GXM for 40 min. The concentration of GXM was chosen based on results from TEER and HBEC barrier permeability experiments. A stock solution of GXM was made by dissolving the polysaccharide in distilled water and further diluted in Krebs solution. A vehicle consisting of distilled water was used as a control (untreated). After treatment, SMA rings were mounted in a Multi-Wire Myograph System 620M (Danish Myo Technology) for isometric tension recordings using a PowerLab 8/35 data acquisition system (ADInstruments Pty Ltd.). SMA rings were equilibrated in Krebs buffer for 30 min, and in chambers perfused with 5% CO₂ in 95% O₂ at 37°C, as described elsewhere [77]. In all experiments, SMA ring integrity was assessed by stimulation with 120 mM KCl (74.7 mM NaCl, 14.9 mM NaHCO₃, 60 mM KCl, 1.18 mM, KH₂PO₄, 1.17 mM MgSO₄-7H₂O, 1.6 mM CaCl₂-2H₂O, 0.026 mM EDTA, 5.5 mM glucose). To test for the presence of endothelium, segments were contracted with 1 μM phenylephrine (PE) (Sigma); once the vessels reached a stable maximum tension, the vessels were stimulated with 10 μM acetylcholine (ACh) (Sigma), and relaxation was confirmed. For the stock solution, PE and ACh were dissolved in distilled water. SMA that achieved relaxation to ACh were considered to have a preserved endothelium. Cumulative concentration-response curves to ACh (1 nM to 10 μM) and PE (1 nM to 10 μM) were performed on intact SMA rings in the absence or presence of 25 μg/mL of GXM. Endothelium-dependent relaxation was recorded for ACh after maximal precontraction with 1 μM PE.

Statistical analysis

All data were subjected to statistical analysis using Prism 9.4 (GraphPad). Differences in survival rates were analyzed by the log-rank test (Mantel-Cox). *P* values for multiple comparisons were calculated by one-way analysis of variance (ANOVA) and were adjusted by use of the Tukey's post-hoc analysis. *P* values for individual comparisons were calculated using student's or multiple *t*-test analyses. The concentration-response curve for vascular reactivity was log-

transformed, normalized to percent maximal response, and fitted using a nonlinear regression. P values of <0.05 were considered significant.

Supporting information

S1 Fig. Exogenous GXM administration 24 h prior to cryptococcal infection causes inflammation of the pulmonary tissue. Representative lung sections (scale bar in 10-100X magnifications: 50 μm) excised from untreated (upper panels) and GXM (125 $\mu\text{g}/\text{mL}$; lower panels)-treated mice, stained with H&E, and sequentially examined under light microscopy are shown. Rectangles in the lobe, 10, 20, and 40X images indicate the lung region magnified in the following picture (on the right).

(TIF)

S2 Fig. *C. neoformans* GXM released in organs and serum of C57BL/6 mice i.t. infected 3- and 7-dpi. Bars and error bars denote the mean value and SDs, respectively. Each symbol represents the value for 1 mouse ($n = 8$ per group).

(TIF)

S3 Fig. Quantitative measurements of individual band intensity in WB analysis shown in Fig 5A for (B) actin protein levels using LiCOR Image Studio software. Bars represent the means of 3 independent gel results (black circles) and error bars indicate SDs. P -value significance ($P < 0.05$) was calculated using one-way ANOVA and adjusted using the Tukey's post-hoc analysis. No statistical difference was found.

(TIF)

S4 Fig. Pericytes increase TEER and strengthen the *in vitro* BBB model. HBECs grown in 0.4 μm pore transwell inserts were placed into wells containing media alone (HBECs) or wells containing human primary pericytes (HBECs + pericytes). Bars and error bars denote the means and SDs, respectively. Each symbol denotes a single well measurement ($n = 3$ wells per group). Asterisks indicate P -value significance (** $P < 0.01$) calculated using student's t -test analysis.

(TIF)

S5 Fig. Minimal GXM concentration required for compromising the BBB integrity. Dose-response curve: Relative TEER of HBECs incubated with purified GXM (0.001, 0.01, 1, 10, 50, or 100 $\mu\text{g}/\text{mL}$) for 2 h at 37°C and 5% CO_2 was performed. HBECs were treated with a mock extract from acapsular strain *cap59* and used as a negative control. Data points are averages of three different TEER measurements ($n = 3$ wells per group per experiment) and error bars denote SDs.

(TIF)

Author Contributions

Conceptualization: Michael R. Does, Luis R. Martinez.

Data curation: Hiu Ham Lee, Mohamed F. Hamed, Maria A. Carrillo-Sepulveda, Michael R. Does, Luis R. Martinez.

Formal analysis: Hiu Ham Lee, Dylan J. Carmichael, Melissa E. Munzen, Mohamed F. Hamed, Rikki B. Rooklin, Maria A. Carrillo-Sepulveda, Michael R. Does, Luis R. Martinez.

Funding acquisition: Eliseo A. Eugenin, Michael R. Does, Luis R. Martinez.

Investigation: Hiu Ham Lee, Dylan J. Carmichael, Victoria Ribeiro, Dana N. Parisi, Melissa E. Munzen, Claudia L. Charles-Niño, Mohamed F. Hamed, Ettiman Kaur, Ayush Mishra, Jiya Patel, Rikki B. Rooklin, Amina Sher, Maria A. Carrillo-Sepulveda.

Methodology: Hiu Ham Lee, Dylan J. Carmichael, Melissa E. Munzen, Claudia L. Charles-Niño, Mohamed F. Hamed, Rikki B. Rooklin, Maria A. Carrillo-Sepulveda, Eliseo A. Eugenin, Michael R. Does, Luis R. Martinez.

Project administration: Eliseo A. Eugenin, Michael R. Does, Luis R. Martinez.

Resources: Claudia L. Charles-Niño, Eliseo A. Eugenin, Michael R. Does, Luis R. Martinez.

Software: Luis R. Martinez.

Supervision: Maria A. Carrillo-Sepulveda, Eliseo A. Eugenin, Michael R. Does, Luis R. Martinez.

Validation: Claudia L. Charles-Niño, Michael R. Does.

Visualization: Victoria Ribeiro, Mohamed F. Hamed, Rikki B. Rooklin, Eliseo A. Eugenin, Michael R. Does.

Writing – original draft: Hiu Ham Lee, Dylan J. Carmichael, Victoria Ribeiro, Dana N. Parisi, Melissa E. Munzen, Mohamed F. Hamed, Ettiman Kaur, Ayush Mishra, Jiya Patel, Rikki B. Rooklin, Amina Sher, Maria A. Carrillo-Sepulveda, Eliseo A. Eugenin, Michael R. Does, Luis R. Martinez.

Writing – review & editing: Melissa E. Munzen, Michael R. Does, Luis R. Martinez.

References

1. Rajasingham R, Smith RM, Park BJ, Jarvis JN, Govender NP, Chiller TM, et al. Global burden of disease of HIV-associated cryptococcal meningitis: an updated analysis. *Lancet Infect Dis.* 2017; 17(8):873–81. Epub 2017/05/10. [https://doi.org/10.1016/S1473-3099\(17\)30243-8](https://doi.org/10.1016/S1473-3099(17)30243-8) PMID: 28483415; PubMed Central PMCID: PMC5818156.
2. Goldman DL, Khine H, Abadi J, Lindenbergh DJ, Pirofski L, Niang R, et al. Serologic evidence for *Cryptococcus neoformans* infection in early childhood. *Pediatrics.* 2001; 107(5):E66. Epub 2001/05/23. <https://doi.org/10.1542/peds.107.5.e66> PMID: 11331716.
3. Levitz SM. The ecology of *Cryptococcus neoformans* and the epidemiology of cryptococcosis. *Rev Infect Dis.* 1991; 13(6):1163–9. Epub 1991/11/01. <https://doi.org/10.1093/clinids/13.6.1163> PMID: 1775849.
4. Neilson JB, Fromtling RA, Bulmer GS. *Cryptococcus neoformans*: size range of infectious particles from aerosolized soil. *Infect Immun.* 1977; 17(3):634–8. Epub 1977/09/01. <https://doi.org/10.1128/iai.17.3.634-638.1977> PMID: 332630; PubMed Central PMCID: PMC421174.
5. Dromer F, Mathoulin-Pelissier S, Launay O, Lortholary O, French Cryptococcosis Study G. Determinants of disease presentation and outcome during cryptococcosis: the CryptoA/D study. *PLoS Med.* 2007; 4(2):e21. Epub 2007/02/08. <https://doi.org/10.1371/journal.pmed.0040021> PMID: 17284154; PubMed Central PMCID: PMC1808080.
6. Lortholary O, Improvisi L, Rayhane N, Gray F, Fitting C, Cavallion JM, et al. Cytokine profiles of AIDS patients are similar to those of mice with disseminated *Cryptococcus neoformans* infection. *Infect Immun.* 1999; 67(12):6314–20. Epub 1999/11/24. <https://doi.org/10.1128/IAI.67.12.6314-6320.1999> PMID: 10569743; PubMed Central PMCID: PMC97035.
7. Chretien F, Lortholary O, Kansau I, Neuville S, Gray F, Dromer F. Pathogenesis of cerebral *Cryptococcus neoformans* infection after fungemia. *J Infect Dis.* 2002; 186(4):522–30. Epub 2002/08/27. <https://doi.org/10.1086/341564> PMID: 12195380.
8. Chang YC, Stins MF, McCaffery MJ, Miller GF, Pare DR, Dam T, et al. Cryptococcal yeast cells invade the central nervous system via transcellular penetration of the blood-brain barrier. *Infect Immun.* 2004; 72(9):4985–95. Epub 2004/08/24. <https://doi.org/10.1128/IAI.72.9.4985-4995.2004> PMID: 15321990; PubMed Central PMCID: PMC517459.

9. Littman ML. Capsule synthesis by *Cryptococcus neoformans*. *Trans N Y Acad Sci*. 1958; 20(7):623–48. Epub 1958/05/01. <https://doi.org/10.1111/j.2164-0947.1958.tb00625.x> PMID: 13556861.
10. Littman ML, Tsubura E. Effect of degree of encapsulation upon virulence of *Cryptococcus neoformans*. *Proc Soc Exp Biol Med*. 1959; 101:773–7. Epub 1959/08/01. <https://doi.org/10.3181/00379727-101-25090> PMID: 14417558.
11. Neilson JB, Ivey MH, Bulmer GS. *Cryptococcus neoformans*: pseudohyphal forms surviving culture with *Acanthamoeba polyphaga*. *Infect Immun*. 1978; 20(1):262–6. Epub 1978/04/01. <https://doi.org/10.1128/iai.20.1.262-266.1978> PMID: 352931; PubMed Central PMCID: PMC421581.
12. Fromtling RA, Shadomy HJ, Jacobson ES. Decreased virulence in stable, acapsular mutants of *cryptococcus neoformans*. *Mycopathologia*. 1982; 79(1):23–9. Epub 1982/07/23. <https://doi.org/10.1007/BF00636177> PMID: 6750405.
13. Cherniak R, Sundstrom JB. Polysaccharide antigens of the capsule of *Cryptococcus neoformans*. *Infect Immun*. 1994; 62(5):1507–12. Epub 1994/05/01. <https://doi.org/10.1128/iai.62.5.1507-1512.1994> PMID: 8168912; PubMed Central PMCID: PMC186341.
14. Goldman DL, Lee SC, Casadevall A. Tissue localization of *Cryptococcus neoformans* glucuronoxylomannan in the presence and absence of specific antibody. *Infect Immun*. 1995; 63(9):3448–53. Epub 1995/09/01. <https://doi.org/10.1128/iai.63.9.3448-3453.1995> PMID: 7642276; PubMed Central PMCID: PMC173475.
15. Vecchiarelli A. Immunoregulation by capsular components of *Cryptococcus neoformans*. *Med Mycol*. 2000; 38(6):407–17. Epub 2001/02/24. <https://doi.org/10.1080/mmy.38.6.407.417> PMID: 11204878.
16. Pettoello-Mantovani M, Casadevall A, Smarnworawong P, Goldstein H. Enhancement of HIV type 1 infectivity in vitro by capsular polysaccharide of *Cryptococcus neoformans* and *Haemophilus influenzae*. *AIDS Res Hum Retroviruses*. 1994; 10(9):1079–87. Epub 1994/09/01. <https://doi.org/10.1089/aid.1994.10.1079> PMID: 7826695.
17. Lee SC, Casadevall A. Polysaccharide antigen in brain tissue of AIDS patients with cryptococcal meningitis. *Clin Infect Dis*. 1996; 23(1):194–5. Epub 1996/07/01. <https://doi.org/10.1093/clinids/23.1.194> PMID: 8816161.
18. Hirase T, Kawashima S, Wong EY, Ueyama T, Rikitake Y, Tsukita S, et al. Regulation of tight junction permeability and occludin phosphorylation by RhoA-p160ROCK-dependent and -independent mechanisms. *J Biol Chem*. 2001; 276(13):10423–31. Epub 2001/01/15. <https://doi.org/10.1074/jbc.M007136200> PMID: 11139571.
19. Peng J, He F, Zhang C, Deng X, Yin F. Protein kinase C- α signals P115RhoGEF phosphorylation and RhoA activation in TNF- α -induced mouse brain microvascular endothelial cell barrier dysfunction. *J Neuroinflammation*. 2011; 8:28. Epub 2011/04/09. <https://doi.org/10.1186/1742-2094-8-28> PMID: 21473788; PubMed Central PMCID: PMC3080812.
20. DeOre BJ, Tran KA, Andrews AM, Ramirez SH, Galie PA. SARS-CoV-2 Spike Protein Disrupts Blood-Brain Barrier Integrity via RhoA Activation. *J Neuroimmune Pharmacol*. 2021; 16(4):722–8. Epub 2021/10/24. <https://doi.org/10.1007/s11481-021-10029-0> PMID: 34687399; PubMed Central PMCID: PMC8536479.
21. Kozel TR, Gullely WF, Cazin J Jr, Immune response to *Cryptococcus neoformans* soluble polysaccharide: immunological unresponsiveness. *Infect Immun*. 1977; 18(3):701–7. Epub 1977/12/01. <https://doi.org/10.1128/iai.18.3.701-707.1977> PMID: 338489; PubMed Central PMCID: PMC421292.
22. Sobel RA, Mitchell ME, Fondren G. Intercellular adhesion molecule-1 (ICAM-1) in cellular immune reactions in the human central nervous system. *Am J Pathol*. 1990; 136(6):1309–16. Epub 1990/06/01. PMID: 1972610; PubMed Central PMCID: PMC1877574.
23. Rubin LL, Staddon JM. The cell biology of the blood-brain barrier. *Annu Rev Neurosci*. 1999; 22:11–28. Epub 1999/04/15. <https://doi.org/10.1146/annurev.neuro.22.1.11> PMID: 10202530.
24. Tsukita S, Furuse M. Occludin and claudins in tight-junction strands: leading or supporting players? *Trends Cell Biol*. 1999; 9(7):268–73. Epub 1999/06/17. [https://doi.org/10.1016/s0962-8924\(99\)01578-0](https://doi.org/10.1016/s0962-8924(99)01578-0) PMID: 10370242.
25. Mukherjee S, Lee S, Mukherjee J, Scharff MD, Casadevall A. Monoclonal antibodies to *Cryptococcus neoformans* capsular polysaccharide modify the course of intravenous infection in mice. *Infect Immun*. 1994; 62(3):1079–88. Epub 1994/03/01. <https://doi.org/10.1128/iai.62.3.1079-1088.1994> PMID: 8112842; PubMed Central PMCID: PMC186227.
26. Zaragoza O, Alvarez M, Telzak A, Rivera J, Casadevall A. The relative susceptibility of mouse strains to pulmonary *Cryptococcus neoformans* infection is associated with pleiotropic differences in the immune response. *Infect Immun*. 2007; 75(6):2729–39. Epub 2007/03/21. <https://doi.org/10.1128/IAI.00094-07> PMID: 17371865; PubMed Central PMCID: PMC1932903.
27. Cohen CJ, Shieh JT, Pickles RJ, Okegawa T, Hsieh JT, Bergelson JM. The coxsackievirus and adenovirus receptor is a transmembrane component of the tight junction. *Proc Natl Acad Sci U S A*. 2001; 98

- (26):15191–6. Epub 2001/12/06. <https://doi.org/10.1073/pnas.261452898> PMID: 11734628; PubMed Central PMCID: PMC65005.
28. Kim JC, Crary B, Chang YC, Kwon-Chung KJ, Kim KJ. Cryptococcus neoformans activates RhoGTPase proteins followed by protein kinase C, focal adhesion kinase, and ezrin to promote traversal across the blood-brain barrier. *J Biol Chem*. 2012; 287(43):36147–57. Epub 2012/08/18. <https://doi.org/10.1074/jbc.M112.389676> PMID: 22898813; PubMed Central PMCID: PMC3476282.
 29. Chen CP, Chen X, Qiao YN, Wang P, He WQ, Zhang CH, et al. In vivo roles for myosin phosphatase targeting subunit-1 phosphorylation sites T694 and T852 in bladder smooth muscle contraction. *J Physiol*. 2015; 593(3):681–700. Epub 2014/11/30. <https://doi.org/10.1113/jphysiol.2014.283853> PMID: 25433069; PubMed Central PMCID: PMC4324713.
 30. Ruiz-Loredo AY, Lopez E, Lopez-Colome AM. Thrombin promotes actin stress fiber formation in RPE through Rho/ROCK-mediated MLC phosphorylation. *J Cell Physiol*. 2011; 226(2):414–23. Epub 2010/07/31. <https://doi.org/10.1002/jcp.22347> PMID: 20672289.
 31. Dalkara T, Gursoy-Ozdemir Y, Yemisci M. Brain microvascular pericytes in health and disease. *Acta Neuropathol*. 2011; 122(1):1–9. Epub 2011/06/10. <https://doi.org/10.1007/s00401-011-0847-6> PMID: 21656168.
 32. Hamed MF, Enriquez V, Munzen ME, Charles-Nino CL, Mihu MR, Khoshbouei H, et al. Clinical and pathological characterization of Central Nervous System cryptococcosis in an experimental mouse model of stereotaxic intracerebral infection. *PLoS Negl Trop Dis*. 2023; 17(1):e0011068. Epub 2023/01/20. <https://doi.org/10.1371/journal.pntd.0011068> PMID: 36656900; PubMed Central PMCID: PMC9888703.
 33. Eng R, Chmel H, Corrado M, Smith SM. The course of cryptococcal capsular polysaccharide antigenemia/human cryptococcal polysaccharide elimination kinetics. *Infection*. 1983; 11(3):132–6. Epub 1983/05/01. <https://doi.org/10.1007/BF01641291> PMID: 6350190.
 34. Lendvai N, Casadevall A, Liang Z, Goldman DL, Mukherjee J, Zuckier L. Effect of immune mechanisms on the pharmacokinetics and organ distribution of cryptococcal polysaccharide. *J Infect Dis*. 1998; 177(6):1647–59. Epub 1998/06/02. <https://doi.org/10.1086/515329> PMID: 9607845.
 35. Muchmore HG, Scott EN, Felton FG, Fromtling RA. Cryptococcal capsular polysaccharide clearance in nonimmune mice. *Mycopathologia*. 1982; 78(1):41–5. Epub 1982/04/23. <https://doi.org/10.1007/BF00436580> PMID: 7048100.
 36. Merkel GJ, Scofield BA. The in vitro interaction of *Cryptococcus neoformans* with human lung epithelial cells. *FEMS Immunol Med Microbiol*. 1997; 19(3):203–13. Epub 1998/02/07. <https://doi.org/10.1111/j.1574-695X.1997.tb01089.x> PMID: 9453390.
 37. Ganendren R, Carter E, Sorrell T, Widmer F, Wright L. Phospholipase B activity enhances adhesion of *Cryptococcus neoformans* to a human lung epithelial cell line. *Microbes Infect*. 2006; 8(4):1006–15. Epub 2006/02/21. <https://doi.org/10.1016/j.micinf.2005.10.018> PMID: 16487740.
 38. Teixeira PA, Penha LL, Mendonca-Previato L, Previato JO. Mannoprotein MP84 mediates the adhesion of *Cryptococcus neoformans* to epithelial lung cells. *Front Cell Infect Microbiol*. 2014; 4:106. Epub 2014/09/06. <https://doi.org/10.3389/fcimb.2014.00106> PMID: 25191644; PubMed Central PMCID: PMC4137752.
 39. Silveira CP, Piffer AC, Kmetzsch L, Fonseca FL, Soares DA, Staats CC, et al. The heat shock protein (Hsp) 70 of *Cryptococcus neoformans* is associated with the fungal cell surface and influences the interaction between yeast and host cells. *Fungal Genet Biol*. 2013; 60:53–63. Epub 2013/08/21. <https://doi.org/10.1016/j.fgb.2013.08.005> PMID: 23954835.
 40. Martinez LR, Casadevall A. Specific antibody can prevent fungal biofilm formation and this effect correlates with protective efficacy. *Infect Immun*. 2005; 73(10):6350–62. Epub 2005/09/24. <https://doi.org/10.1128/IAI.73.10.6350-6362.2005> PMID: 16177306; PubMed Central PMCID: PMC1230912.
 41. Taylor-Smith LM. *Cryptococcus-Epithelial Interactions*. *J Fungi (Basel)*. 2017; 3(4). Epub 2018/01/27. <https://doi.org/10.3390/jof3040053> PMID: 29371569; PubMed Central PMCID: PMC5753155.
 42. Nakouzi A, Zhang T, Oscarson S, Casadevall A. The common *Cryptococcus neoformans* glucuronoxylomannan M2 motif elicits non-protective antibodies. *Vaccine*. 2009; 27(27):3513–8. Epub 2009/05/26. <https://doi.org/10.1016/j.vaccine.2009.03.089> PMID: 19464529; PubMed Central PMCID: PMC2932445.
 43. Sato K, Matsumoto I, Suzuki K, Tamura A, Shiraishi A, Kiyonari H, et al. Deficiency of lung-specific claudin-18 leads to aggravated infection with *Cryptococcus neoformans* through dysregulation of the microenvironment in lungs. *Sci Rep*. 2021; 11(1):21110. Epub 2021/10/28. <https://doi.org/10.1038/s41598-021-00708-6> PMID: 34702961; PubMed Central PMCID: PMC8548597.
 44. Ellerbroek PM, Hoepelman AI, Wolbers F, Zwaginga JJ, Coenjaerts FE. Cryptococcal glucuronoxylomannan inhibits adhesion of neutrophils to stimulated endothelium in vitro by affecting both neutrophils

- and endothelial cells. *Infect Immun*. 2002; 70(9):4762–71. Epub 2002/08/17. <https://doi.org/10.1128/IAI.70.9.4762-4771.2002> PMID: 12183517; PubMed Central PMCID: PMC128235.
45. Ellerbroek PM, Ulfman LH, Hoepelman AI, Coenjaerts FE. Cryptococcal glucuronoxylomannan interferes with neutrophil rolling on the endothelium. *Cell Microbiol*. 2004; 6(6):581–92. Epub 2004/04/24. <https://doi.org/10.1111/j.1462-5822.2004.00384.x> PMID: 15104598.
 46. Gibson JF, Bojarczuk A, Evans RJ, Kamuyango AA, Hotham R, Lagendijk AK, et al. Blood vessel occlusion by *Cryptococcus neoformans* is a mechanism for haemorrhagic dissemination of infection. *PLoS Pathog*. 2022; 18(4):e1010389. Epub 2022/04/22. <https://doi.org/10.1371/journal.ppat.1010389> PMID: 35446924; PubMed Central PMCID: PMC9022829.
 47. Li X, Liu G, Ma J, Zhou L, Zhang Q, Gao L. Lack of IL-6 increases blood-brain barrier permeability in fungal meningitis. *J Biosci*. 2015; 40(1):7–12. Epub 2015/03/06. <https://doi.org/10.1007/s12038-014-9496-y> PMID: 25740137.
 48. Olszewski MA, Noverr MC, Chen GH, Toews GB, Cox GM, Perfect JR, et al. Urease expression by *Cryptococcus neoformans* promotes microvascular sequestration, thereby enhancing central nervous system invasion. *Am J Pathol*. 2004; 164(5):1761–71. Epub 2004/04/28. [https://doi.org/10.1016/S0002-9440\(10\)63734-0](https://doi.org/10.1016/S0002-9440(10)63734-0) PMID: 15111322; PubMed Central PMCID: PMC1615675.
 49. Subramaniam KS, Datta K, Quintero E, Manix C, Marks MS, Pirofski LA. The absence of serum IgM enhances the susceptibility of mice to pulmonary challenge with *Cryptococcus neoformans*. *J Immunol*. 2010; 184(10):5755–67. Epub 2010/04/21. <https://doi.org/10.4049/jimmunol.0901638> PMID: 20404271; PubMed Central PMCID: PMC2885446.
 50. Bennett JE, Hasenclever HF. *Cryptococcus Neoformans* Polysaccharide: Studies of Serologic Properties and Role in Infection. *J Immunol*. 1965; 94:916–20. Epub 1965/06/01. PMID: 14321434.
 51. Coelho C, Camacho E, Salas A, Alanio A, Casadevall A. Intranasal Inoculation of *Cryptococcus neoformans* in Mice Produces Nasal Infection with Rapid Brain Dissemination. *mSphere*. 2019; 4(4). Epub 2019/08/09. <https://doi.org/10.1128/mSphere.00483-19> PMID: 31391283; PubMed Central PMCID: PMC6686232.
 52. Nakae Y, Kudo Y, Yamamoto R, Johkura K. Pseudo-subarachnoid hemorrhage in cryptococcal meningitis: MRI findings and pathological study. *Neurol Sci*. 2013; 34(12):2227–9. Epub 2013/05/25. <https://doi.org/10.1007/s10072-013-1461-2> PMID: 23703398.
 53. Shimoda Y, Ohtomo S, Arai H, Ohtoh T, Tominaga T. Subarachnoid small vein occlusion due to inflammatory fibrosis—a possible mechanism for cerebellar infarction in cryptococcal meningoencephalitis: a case report. *BMC Neurol*. 2017; 17(1):157. Epub 2017/08/11. <https://doi.org/10.1186/s12883-017-0934-y> PMID: 28793877; PubMed Central PMCID: PMC5551018.
 54. Lofgren S, Hullsiek KH, Morawski BM, Nabeta HW, Kiggundu R, Taseera K, et al. Differences in Immunologic Factors Among Patients Presenting with Altered Mental Status During Cryptococcal Meningitis. *J Infect Dis*. 2017; 215(5):693–7. Epub 2017/03/23. <https://doi.org/10.1093/infdis/jix033> PMID: 28329080; PubMed Central PMCID: PMC5388270.
 55. Song W, Shen YZ, Wang ZY, Qi TK, Liu L, Zhang RF, et al. Clinical features and treatment outcomes of human immunodeficiency virus-associated cryptococcal meningitis: a 2-year retrospective analysis. *Chin Med J (Engl)*. 2020; 133(23):2787–95. Epub 2020/12/05. <https://doi.org/10.1097/CM9.0000000000001191> PMID: 33273326; PubMed Central PMCID: PMC7717751.
 56. Chen SHM, Stins MF, Huang SH, Chen YH, Kwon-Chung KJ, Chang Y, et al. *Cryptococcus neoformans* induces alterations in the cytoskeleton of human brain microvascular endothelial cells. *J Med Microbiol*. 2003; 52(Pt 11):961–70. Epub 2003/10/09. <https://doi.org/10.1099/jmm.0.05230-0> PMID: 14532340.
 57. Suzuki Y, Yamamoto M, Wada H, Ito M, Nakano T, Sasaki Y, et al. Agonist-induced regulation of myosin phosphatase activity in human platelets through activation of Rho-kinase. *Blood*. 1999; 93(10):3408–17. Epub 1999/05/11. PMID: 10233893.
 58. Carbajal JM, Gratrix ML, Yu CH, Schaeffer RC Jr, ROCK mediates thrombin's endothelial barrier dysfunction. *Am J Physiol Cell Physiol*. 2000; 279(1):C195–204. Epub 2000/07/18. <https://doi.org/10.1152/ajpcell.2000.279.1.C195> PMID: 10898731.
 59. Eugenin EA, Greco JM, Frases S, Nosanchuk JD, Martinez LR. Methamphetamine alters blood brain barrier protein expression in mice, facilitating central nervous system infection by neurotropic *Cryptococcus neoformans*. *J Infect Dis*. 2013; 208(4):699–704. Epub 2013/03/28. <https://doi.org/10.1093/infdis/jit117> PMID: 23532099; PubMed Central PMCID: PMC3719895.
 60. Santiago-Tirado FH, Onken MD, Cooper JA, Klein RS, Doering TL. Trojan Horse Transit Contributes to Blood-Brain Barrier Crossing of a Eukaryotic Pathogen. *mBio*. 2017; 8(1). Epub 2017/02/02. <https://doi.org/10.1128/mBio.02183-16> PMID: 28143979; PubMed Central PMCID: PMC5285505.
 61. Tseng HK, Liu CP, Price MS, Jong AY, Chang JC, Toffaletti DL, et al. Identification of genes from the fungal pathogen *Cryptococcus neoformans* related to transmigration into the central nervous system.

- PLoS One. 2012; 7(9):e45083. Epub 2012/10/03. <https://doi.org/10.1371/journal.pone.0045083> PMID: [23028773](https://pubmed.ncbi.nlm.nih.gov/23028773/); PubMed Central PMCID: PMC3447876.
62. Vu K, Tham R, Uhrig JP, Thompson GR 3rd, Na Pombejra S, Jamklang M, et al. Invasion of the central nervous system by *Cryptococcus neoformans* requires a secreted fungal metalloprotease. *mBio*. 2014; 5(3):e01101–14. Epub 2014/06/05. <https://doi.org/10.1128/mBio.01101-14> PMID: [24895304](https://pubmed.ncbi.nlm.nih.gov/24895304/); PubMed Central PMCID: PMC4049100.
 63. Vu K, Weksler B, Romero I, Couraud PO, Gelli A. Immortalized human brain endothelial cell line HCMEC/D3 as a model of the blood-brain barrier facilitates in vitro studies of central nervous system infection by *Cryptococcus neoformans*. *Eukaryot Cell*. 2009; 8(11):1803–7. Epub 2009/09/22. <https://doi.org/10.1128/EC.00240-09> PMID: [19767445](https://pubmed.ncbi.nlm.nih.gov/19767445/); PubMed Central PMCID: PMC2772405.
 64. Armulik A, Genove G, Mae M, Nisancioglu MH, Wallgard E, Niaudet C, et al. Pericytes regulate the blood-brain barrier. *Nature*. 2010; 468(7323):557–61. Epub 2010/10/15. <https://doi.org/10.1038/nature09522> PMID: [20944627](https://pubmed.ncbi.nlm.nih.gov/20944627/).
 65. Nielson JA, Davis JM. Roles for Microglia in Cryptococcal Brain Dissemination in the Zebrafish Larva. *Microbiol Spectr*. 2023:e0431522. Epub 2023/02/01. <https://doi.org/10.1128/spectrum.04315-22> PMID: [36719205](https://pubmed.ncbi.nlm.nih.gov/36719205/).
 66. Kilkenny C, Browne WJ, Cuthill IC, Emerson M, Altman DG. Improving bioscience research reporting: the ARRIVE guidelines for reporting animal research. *PLoS Biol*. 2010; 8(6):e1000412. Epub 2010/07/09. <https://doi.org/10.1371/journal.pbio.1000412> PMID: [20613859](https://pubmed.ncbi.nlm.nih.gov/20613859/); PubMed Central PMCID: PMC2893951.
 67. Garcia-Rivera J, Chang YC, Kwon-Chung KJ, Casadevall A. *Cryptococcus neoformans* CAP59 (or Cap59p) is involved in the extracellular trafficking of capsular glucuronoxylomannan. *Eukaryot Cell*. 2004; 3(2):385–92. <https://doi.org/10.1128/EC.3.2.385-392.2004> PMID: [15075268](https://pubmed.ncbi.nlm.nih.gov/15075268/); PubMed Central PMCID: PMC387637.
 68. Nimrichter L, Frases S, Cinelli LP, Viana NB, Nakouzi A, Travassos LR, et al. Self-aggregation of *Cryptococcus neoformans* capsular glucuronoxylomannan is dependent on divalent cations. *Eukaryot Cell*. 2007; 6(8):1400–10. Epub 2007/06/19. <https://doi.org/10.1128/EC.00122-07> PMID: [17573547](https://pubmed.ncbi.nlm.nih.gov/17573547/); PubMed Central PMCID: PMC1951138.
 69. Casadevall A, Mukherjee J, Scharff MD. Monoclonal antibody based ELISAs for cryptococcal polysaccharide. *J Immunol Methods*. 1992; 154(1):27–35. Epub 1992/09/18. [https://doi.org/10.1016/0022-1759\(92\)90209-c](https://doi.org/10.1016/0022-1759(92)90209-c) PMID: [1401941](https://pubmed.ncbi.nlm.nih.gov/1401941/).
 70. Dische Z. A specific color reaction for glucuronic acid. *J Biol Chem*. 1947; 171(2):725–30. Epub 1947/12/01. PMID: [20272112](https://pubmed.ncbi.nlm.nih.gov/20272112/).
 71. Dubois M, Gilles K, Hamilton JK, Rebers PA, Smith F. A colorimetric method for the determination of sugars. *Nature*. 1951; 168(4265):167. Epub 1951/07/28. <https://doi.org/10.1038/168167a0> PMID: [14875032](https://pubmed.ncbi.nlm.nih.gov/14875032/).
 72. Martinez LR, Moussai D, Casadevall A. Antibody to *Cryptococcus neoformans* glucuronoxylomannan inhibits the release of capsular antigen. *Infect Immun*. 2004; 72(6):3674–9. Epub 2004/05/25. <https://doi.org/10.1128/IAI.72.6.3674-3679.2004> PMID: [15155683](https://pubmed.ncbi.nlm.nih.gov/15155683/); PubMed Central PMCID: PMC415713.
 73. Martinez LR, Mihu MR, Han G, Frases S, Cordero RJ, Casadevall A, et al. The use of chitosan to damage *Cryptococcus neoformans* biofilms. *Biomaterials*. 2010; 31(4):669–79. Epub 2009/10/13. <https://doi.org/10.1016/j.biomaterials.2009.09.087> PMID: [19819009](https://pubmed.ncbi.nlm.nih.gov/19819009/); PubMed Central PMCID: PMC2783412.
 74. Castellano P, Nwagbo C, Martinez LR, Eugenin EA. Methamphetamine compromises gap junctional communication in astrocytes and neurons. *J Neurochem*. 2016; 137(4):561–75. Epub 2016/03/10. <https://doi.org/10.1111/jnc.13603> PMID: [26953131](https://pubmed.ncbi.nlm.nih.gov/26953131/); PubMed Central PMCID: PMC5050922.
 75. Hernandez-Santini AC, Mitha AN, Chow D, Hamed MF, Gućwa AL, Vaval V, et al. Methamphetamine facilitates pulmonary and splenic tissue injury and reduces T cell infiltration in C57BL/6 mice after antigenic challenge. *Sci Rep*. 2021; 11(1):8207. Epub 2021/04/17. <https://doi.org/10.1038/s41598-021-87728-4> PMID: [33859291](https://pubmed.ncbi.nlm.nih.gov/33859291/); PubMed Central PMCID: PMC8050260.
 76. Chen HR, Yeh TM. In vitro Assays for Measuring Endothelial Permeability by Transwells and Electrical Impedance Systems. *Bio Protoc*. 2017; 7(9):e2273. Epub 2017/05/05. <https://doi.org/10.21769/BioProtoc.2273> PMID: [34541256](https://pubmed.ncbi.nlm.nih.gov/34541256/); PubMed Central PMCID: PMC8410333.
 77. Carrillo-Sepulveda MA, Ceravolo GS, Furstenau CR, Monteiro Pde S, Bruno-Fortes Z, Carvalho MH, et al. Emerging role of angiotensin type 2 receptor (AT2R)/Akt/NO pathway in vascular smooth muscle cell in the hyperthyroidism. *PLoS One*. 2013; 8(4):e61982. Epub 2013/05/03. <https://doi.org/10.1371/journal.pone.0061982> PMID: [23637941](https://pubmed.ncbi.nlm.nih.gov/23637941/); PubMed Central PMCID: PMC3634851.